Ferrite Rod Antenna in a Nanosatellite Medium and High Frequency Radio

Petri Koskimaa

School of Electrical Engineering

Thesis submitted for examination for the degree of Master of Science in Technology.

Espoo 10.10.2016

Thesis supervisor:

Prof. Esa Kallio

Thesis advisors:

D.Sc. (Tech.) Juha Mallat

M.Sc. Antti Kestilä

Aalto University
School of Electrical
Engineering

AALTO UNIVERSITY
SCHOOL OF ELECTRICAL ENGINEERING

ABSTRACT OF THE
MASTER'S THESIS

Author: Petri Koskimaa

Title: Ferrite Rod Antenna in a Nanosatellite Medium and High Frequency Radio

Date: 10.10.2016 Language: English Number of pages: 10+51

Department of Radio Science and Technology

Professorship: Space Technology and Science

Supervisor: Prof. Esa Kallio

Advisors: D.Sc. (Tech.) Juha Mallat, M.Sc. Antti Kestilä

In this thesis the feasibility of using a ferrite rod antenna as a part of a radio instrument in a nanosatellite was studied. Ferrite rod antennas are used as receiving antennas for amplitude modulation transmissions in the medium and high frequencies. At these frequencies it is possible to study ionospheric properties due to the refraction of radiowaves from different ionospheric layers.
The behavior of the antenna was determined from theory and tested using electromagnetic simulation software and measurements. The aluminium body and other metallic structures in the satellite affect the operation of the antenna and its position must be chosen carefully. The results show that ferrite rod antennas can be used for the purpose of receiving medium and high frequency transmissions in an aluminium framed nanosatellite.

Keywords: medium frequency, high frequency, ferrite rod antenna, nanosatellite

AALTO-YLIOPISTO
SÄHKÖTEKNIIKAN KORKEAKOULU

DIPLOMITYÖN
TIIVISTELMÄ

Tekijä: Petri Koskimaa

Työn nimi: Ferriittiantenni nanosatelliitin keski- ja korkeataajuuksien radiossa

Päivämäärä: 10.10.2016 Kieli: Englanti Sivumäärä: 10+51

Radiotieteen ja -tekniikan laitos

Professuuri: Avaruustekniikka ja -tiede

Työn valvoja: Prof. Esa Kallio

Työn ohjaajat: TkT Juha Mallat, DI Antti Kestilä

Tässä työssä tutkittiin ferriittiantennien käyttöä nanosatelliittiin tulevassa radioinstrumentissa. Ferriittiantenneja käytetään amplitudimodulaatiolähetyksien vastaanottoantenneina keski- ja korkeataajuuksilla. Näillä taajuuksilla ionosfäärin ominaisuuksia voidaan tutkia ionosfäärin eri kerrosten aiheuttamasta radioaaltojen refraktion johtuen.
Antennin toimintaa tarkasteltiin teorian kautta ja se todennettiin sähkömagnetismisimulaatio-ohjelmaa käyttäen sekä mittauksilla. Alumiininen runko sekä muut metallirakenteet satelliitissa vaikuttavat antennin toimintaan ja sen sijoitus tulee tehdä tarkoin. Tulokset näyttävät, että ferriittiantennia voidaan käyttää keski- ja korkeiden taajuuksien vastaanottoantennina alumiinirunkoisessa nanosatelliitissa.

Avainsanat: keskitaajuus, korkeataajuus, ferriittiantenni, nanosatelliitti

Preface

I want to thank my supervisor and advisors. Thanks to family and friends for support.

Otaniemi, 10.10.2016

Petri J. Koskimaa

Contents

Symbols and abbreviations

Symbols

A	area
B	magnetic flux density vector
B	magnetic flux density
B_0	magnetic flux density amplitude
C	capacitance
C_c	coil capacitance
C_m	matching capacitance
C_t	turn-to-turn capacitance
C_0	junction capacitance with no bias
c_0	speed of light in vacuum
D_f	demagnetization factor
D	antenna directivity
E	electric field
e	Euler's number
f	frequency
f_{IF}	intermediate frequency
f_{LO}	local oscillator frequency
f_{RF}	amplitude modulation radio frequency
f_0	resonance frequency
f_o	resonance frequency with secondary winding open
f_s	resonance frequency with secondary winding shorted
G	gain
G_r	receiver gain
G_{real}	realized gain
G_t	transmitter gain
h	septum-to-floor height
h_e	antenna effective height
H	magnetic field
H_0	magnetic field amplitude
I_1	primary circuit current
I_2	secondary circuit current
j	imaginary unit
K	coil coefficient
k	coupling coefficient
L	inductance
l_c	coil length
L_f	ferrite rod inductance
l_f	ferrite rod length
L_{fs}	free-space path loss
L_s	primary winding inductance with secondary winding shorted
l_w	wire length
L_1	primary winding inductance
L_2	secondary winding inductance

Symbols

M	mutual impedance
m_e	electron mass
N	number of turns in a coil
n	junction doping profile exponent
N_1	primary winding number of turns
N_2	secondary winding number of turns
n_e	number density of electrons
P_{in}	antenna input power
P_{loss}	power loss
P_r	received power
P_{rad}	radiated power
P_t	transmitted power
Q	quality factor
q	electric charge
R	resistance
r	distance
R_A	antenna resistance
R_{LD}	core length-to-diameter ratio
R_c	capacitor loss resistance
r_c	coil radius
R_{excess}	excess resistance
R_f	ferrite core loss resistance
r_f	ferrite rod radius
R_i	inductor loss resistance
R_{loss}	loss resistance
R_p	coil loss with proximity effect
R_r	radiation resistance
R_s	conductor surface resistance
R_w	wire resistance
r_w	wire radius
R_0	coil loss without proximity effect
S	power density
S	scattering matrix
t	time
$\tan \delta_m$	magnetic loss tangent
U	voltage
U_{coil}	induced electromotive force in the coil
U_0	junction voltage with no bias
U_1	voltage in the primary winding
U_2	voltage in the secondary winding
W_e	average electric energy
W_m	average magnetic energy
X	reactance
X_A	antenna reactance
Z_A	antenna impedance
Z_C	parallel capacitor impedance
Z_L	coil impedance
Z_0	impedance of free space
Z_1	primary circuit impedance
Z_2	secondary circuit impedance

Symbols

Γ	reflection coefficient
δ	skin depth
Δf	bandwidth
ϵ_r	relative permittivity
ϵ_0	vacuum permittivity
η_r	radiation efficiency
η_t	total efficiency
θ	polar angle
λ	wavelength
μ_e	effective permeability
μ_r	relative permeability
μ_0	vacuum permeability
π	pi
σ	conductivity
Φ	magnetic flux
ϕ	azimuth angle
ω	angular frequency

Abbreviations

AM	amplitude modulation
BNC	Bayonet Neill-Concelman
COSPAR	Committee on Space Research
COTS	commercial-off-the-shelf
CST	Computer Simulation Technology
CST MWS	Computer Simulation Technology Microwave Studio
DC	direct current
DUT	device under test
EMF	electromotive force
ESA	European Space Agency
GTEM	gigahertz transverse electromagnetic
HF	high frequency
HUTSAT	Helsinki University of Technology Satellite
IC	integrated circuit
ITU	International Telecommunications Union
ITU-R	International Telecommunications Union Radiocommunication Sector
LF	low frequency
LW	longwave
MF	medium frequency
MW	medium wave
NASA	National Aeronautics and Space Administration
PCB	printed circuit board
QFN	quad flat no-leads
RF	radio frequency
SLL	side-lobe level
SNNR	signal-plus-noise-to-noise-ratio
SNR	signal-to-noise ratio
SW	shortwave
TEM	transverse electromagnetic
UHF	ultra high frequency
UV	ultraviolet

1 Introduction

1.1 Space research in Finland

Finland became a member of the international Committee on Space Research (COSPAR) in 1964. The first satellite with Finnish collaboration was the Soviet Phobos-1 launched in 1988. Around the same time Finland also joined the European Space Agency (ESA) as an associate member in 1987 and as a full member in 1995. [1] Since then Finnish companies and universities have participated in many space projects, both as a member of ESA and also bilaterally with other countries, such as the Rosetta mission launched in 2004 [2].

The first attempt to develop a Finnish satellite was HUTSAT developed in the former Helsinki University of Technology. The project was initiated in 1992 and a flight model was to be built by 1997 [3]. The satellite was never finished but in 2010 Aalto University started a project with the goal to build Finland's first satellite. Named Aalto-1 the satellite is a nanosatellite and has been built as a student project with contributions other institutions such as VTT Technical Research Centre of Finland that provides the main payload [4]. The satellite has been delivered to the launcher and the planned launch is during 2016. Aalto University is also working on two other satellites: Aalto-2 and Suomi 100.

Nanosatellites are satellites with a mass ranging from 1 kg to 10 kg. [5, p. 576] Nanosatellite launch costs are significantly smaller compared to a traditional satellite as their mass is smaller and because of the smaller size multiple nanosatellites can be launched at the same time, even piggyback on a launch for a large satellite. Many commercial-off-the-shelf (COTS) components can be used in space environment [5]. This in addition to easier and faster production make them a lucrative choice for a larger pool of institutions and organization. In recent years they have become a popular platform for satellite missions. Many universities have taken interest in nanosatellites. [5]

CubeSat is a standardized nanosatellite format first proposed in 1998 [5]. All satellites in Aalto University are based on this format. CubeSats consist of cubic units whose outer dimensions are $10 \times 10 \times 10$ cm [5]. Figure 1 depicts a nanosatellite of 2 CubeSat units. It allows a more streamlined and quicker way to develop and launch a satellite as it offers ready solutions and guidelines around which the mission can be based on. As with nanosatellites in general this has allowed new organizations into the space technology and science. Also from the launcher's perspective it is favorable that nanosatellites follow the same standard.

Suomi 100 satellite is part of the centennial of Finland's independence carrying the same name. It is a nanosatellite that will orbit the Earth on a polar orbit at approximately 500 km altitude. Polar orbits are used by remote sensing satellites and other satellites that want to have a coverage of the globe. The satellite has three major purposes: scientific, educational and raising the national spirit. First and foremost it is a scientific satellite that will make observations in Earth's vicinity. The scientific payload consists of a wide angle camera that will image Earth, specifically Finland, and also natural phenomena such as auroras. In addition it has a radio

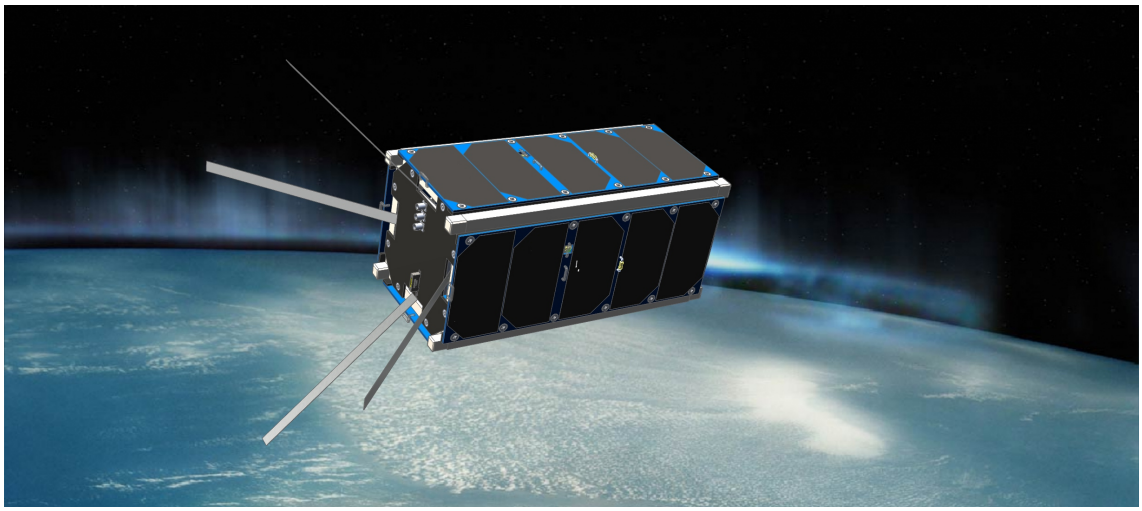

Figure 1: A concept image of a 2-unit CubeSat on orbit. Courtesy of Aalto University.

instrument operating on medium and high frequencies that measures both man-made and natural radio emissions. The satellite is built in Finland so it is giving opportunities for people to gain knowledge and skills in space technology. Suomi 100 satellite can be used as a demonstration of space technology and research and their importance. Lastly the purpose of the satellite is to generate interest in space activities among general public, maintain Finland's position as a high technology country and unite the people of Finland. [6]

1.2 Medium and high frequency environment

The International Telecommunications Union divided the radio spectrum into 12 different frequency bands [7]. In table 1 the relevant frequency bands for AM broadcasting (bands 4 (LF); 5 (MF) and 6 (HF)) are listed. Longwave, medium wave and shortwave are not in official usage but they are still used unofficially as a legacy of early 21th century radio broadcasting. These days they refer to specific AM broadcast frequencies [8]. One way to divide them is given in table 1.

The atmosphere exhibits wavelength areas where the atmosphere is mostly invisible to the electromagnetic radiation as shown in figure 2. These are called windows such as the optical window and radio window. At the frequencies of the radio instrument the most notable man-made emissions are AM broadcasts. These broadcasts are on the edge of the radio window.

AM transmission utilizes the ionospheric properties to achieve very long transmission distances. Ionosphere consists of free electrons and positive ions in an electrically neutral medium [9, p. 1]. The ionosphere causes refraction in electromagnetic waves with lower frequencies refracting more than higher. The electron densities of the ionosphere vary depending on location and time of the day and year. The F2 layer of the ionosphere has the greatest concentration of electrons and is also the most variable and difficult to predict [9, p. 39]. The lower bound in frequency at which

Table 1: ITU-R official designations for frequency bands [7] and commonly used names.

Band name	**Acronym**	**Frequency range**
Low frequency	LF	30 - 300 kHz
Medium frequency	MF	300 - 3000 kHz
High frequency	HF	3 - 30 MHz
Longwave	LW	148.5 - 283.5 kHz (ITU Region 1) < 535 kHz (Longwave Club of America)
Medium wave	MW	526.5 - 1606.5 kHz (Region 1) 535 kHz - 1705 kHz (Region 2)
Shortwave	SW	1.605 - 30 MHz (Region 1) 1.705 - 30 MHz (Region 2)

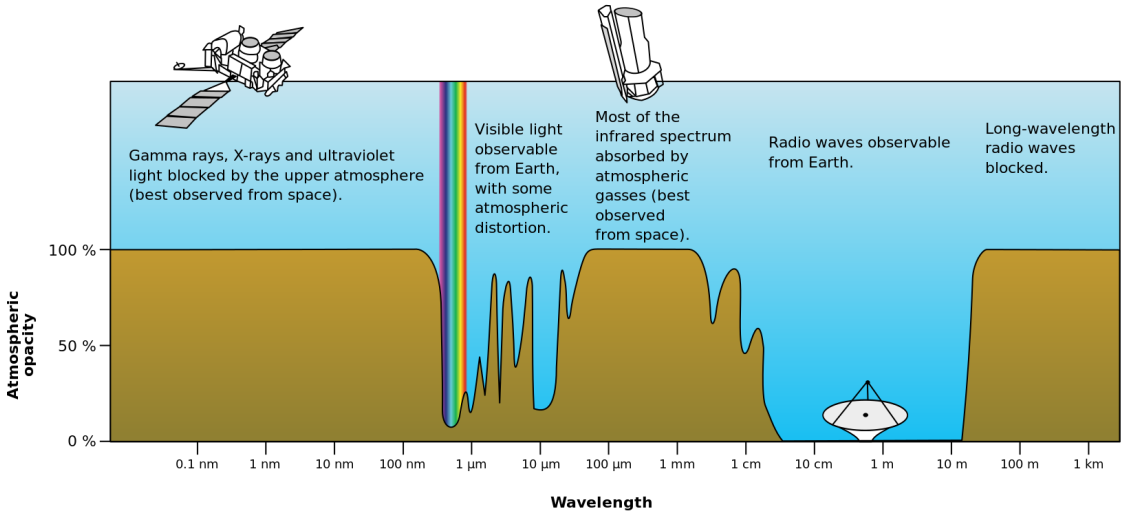

Figure 2: Atmospheric opacity showing visible light and radio windows. Courtesy of NASA.

ordinary electromagnetic waves (O-wave) no longer penetrate the ionospheric F2 layer is denoted as $f_O F2$ frequency [9]. The electron plasma frequency is

$$f = \sqrt{\frac{n_e e^2}{\eta_0 m_e}} \approx 9 \text{ kHz} \sqrt{n_e[cm^{-3}]}, \tag{1}$$

where n_e is number density of electrons, e is the electric charge, and m_e the electron mass. The maximum electron density in the ionosphere is approximately 10^5 – 10^6 cm^{-3}, which according to equation (1) corresponds to a frequency of 3 – 9 MHz. [10] The radio instrument's frequency range should extend to these frequencies to receive signals from Earth.

The variable nature of the RF environment at the studied frequencies is an interesting field of study for which measurements from an instrument on orbit could

provide to be useful. By measuring the electromagnetic radiation originating from Earth it's possible to obtain information about the ionosphere. On the frequencies that reliably penetrate the ionosphere a global radio frequency interference map could be produced.

The lower end of radio spectrum is not well studied with space radio instruments as it has had limited interest compared to other frequency bands. Also the signal wavelength is very large compared to the size of satellites. For example the wavelength of 1 MHz signal is 300 meters. The more common antenna types such as dish and dipole antennas are not feasible and another type of antenna must be used. A possible solution is to use a loop antenna which are used also on Earth to receive signals at these frequencies.

Similarly the natural RF environment on the orbit can be measured. Natural phenomena that are active at low frequencies include for example lightning [11]. The onboard camera instrument will try to image these and theoretically the low frequency emissions from them could be measured as well.

1.3 Research purpose and goals

The purpose of this thesis is to evaluate how a ferrite rod antenna can be implemented in a nanosatellite to use it as a receiving antenna. The satellite will have three antennas onboard to cover a wider frequency range from below 1 MHz up to 6 MHz. Antennas are designed to have a maximal sensitivity and output voltage on their frequency bands.

Due to the size constraints the antennas must be positioned close to each other and the satellite itself and any other instruments it might contain. The signal attenuation and distortion of the frequency response need to be minimized by choosing optimal positions for the antennas.

1.4 Main questions and problems

Nowadays computer simulations have become widely used due to the increased computation speed even with personal computers. This thesis explores how the antenna structures can be simulated with results that are in accordance with both theory and actual measurements.

The main concern for the antenna is how the satellite and its systems and other instruments will affect the performance. Metallic structures nearby the antenna can cause attenuation and change the resonance frequency. This will set constraints on where the antennas can be placed.

1.5 Outlining the scope of research and major concepts

The thesis will focus on the radio front-end, which consists of the ferrite rod antenna and the accompanying circuitry that connects it to the radio receiver. The radio will be built using a commercial integrated circuit by Silicon Laboratories [12]. The

radio circuit needs to be integrated on a printed circuit board which itself needs to be integrated with the satellite.

The main focus is to apply theory into creating realistic simulation models and use them to study how the antennas behave. Supporting measurements with a prototype antenna are done to confirm how accurately the simulations reflect reality. The main test equipment used in measurements was a GTEM cell that can be used as an alternative for many measurements done in an anchoic chamber [13].

By confirming that the simulations are working correctly they can be reused in the future by including any new information regarding the satellite or the radio instrument. These include physical changes in the satellite design and changes in the scientific goals such as addition of new frequencies.

2 Background

An antenna is a device that receives or transmits electromagnetic radiation. Antennas can be divided into four main categories: electrically small antennas, resonant antennas, broadband antennas and aperture antennas [14]. No antenna type is automatically better than the other but the most suitable antenna is determined by the requirements for the specific application. Typical needs for an antenna are for example high gain, narrowband or wideband operation or its physical size.

The fundamental properties and theory of small antennas were well known almost 70 years ago [15] [16]. The ferrite rod antenna is a type of a small magnetic loop antenna. In its simplest form a loop antenna is a single loop of wire to which an external magnetic field induces a voltage according to Faraday's law. In ferrite rod antennas the wire is wound around the ferrite core to form a coil. Both the multi-turn coil and the increased relative permeability inside the coil increase the voltage that can be induced in the antenna from an incident electromagnetic field. [14]

Ferrite rod antennas are used at high frequencies and below as receiving antennas. As the frequency decreases and wavelength increases many common antenna types become impractical in normal usage. For example a half-wave dipole for 1 MHz would have to be 150 meters in length. Ferrite rod antennas are electrically small. Defining properties for an electrically small antenna are low directivity, low input resistance, high input reactance and low radiation efficiency [14, p. 20]. Ferrite rod antennas are not suitable as a transmitting antenna. The power required to radiate any meaningful level of radiation would create enough heat to damage or destroy the antenna [14, p. 60]. Ferrite rod antennas can be used as receivers where this is not a problem.

2.1 Equivalent circuit and antenna impedance

The operation of the antenna can be analyzed by using an equivalent circuit. The ferrite rod antenna consists of a coil which can be modeled as an inductor that has various resistances in series due to the antenna losses. Together with a parallel capacitance the antenna forms a parallel RLC circuit as shown in figure 3. The RLC resonance frequency

$$f_0 = \frac{1}{2\pi\sqrt{LC}} \tag{2}$$

can be tuned by adjusting the capacitance of the capacitor. The impedance seen from the antenna terminals is the antenna impedance:

$$Z_A = R_A + jX_A \tag{3}$$

The antenna impedance needs to be matched to a input impedance of the rest of the circuit. Typically this impedance is 50 Ω.

2.2 Inductance

Loop antennas are inherently inductive where the energy is stored in the magnetic field. The loop resists changes in the current and this is described with an inductance.

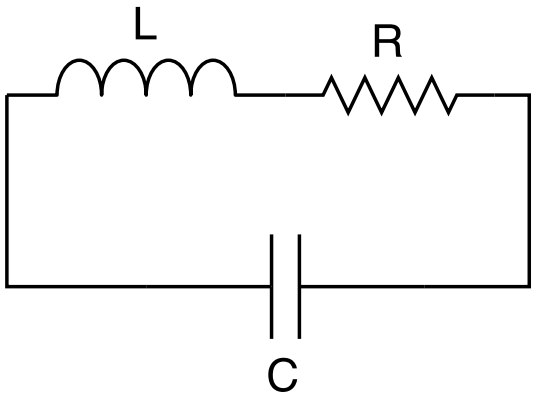

Figure 3: RLC circuit showing the coil inductance (L), resistances (R) including radiation resistance and ohmic losses and parallel capacitance (C).

The inductance of a single-layer air core coil can be approximated [17] [18] as

$$L = \frac{3.133\mu_0 N^2 r_c}{0.9 + l_c/r_c}, \tag{4}$$

where N is the number of coil turns, r_c the coil radius and l_c the coil length. For the ferrite core coil the above formula is not valid. The increased relative permeability of the ferrite material is taken into account and the inductance becomes [19]

$$L_f = \mu_0 \mu_e N^2 \frac{A}{l_f}, \tag{5}$$

where the area $A = \pi r_f^2$ is the ferrite rod cross section with a radius r_f and l_f is the length of the rod. The effective permeability μ_e shouldn't be confused with the relative permeability μ_r, which is the material property of the ferrite core. The effective permeability is dependent on multiple factors: the relative permeability, length and diameter of the rod and the size and position of the coil. The analytical derivation of the relationship between the two permeabilities is cumbersome. An approximation from measurement results for the effective permeability is

$$\mu_e = \frac{\mu_r}{1 + D_f(\mu_r - 1)}, \tag{6}$$

where the demagnetization factor is

$$D_f = 0.37R^{-1.44}, \tag{7}$$

where the core length-to-diameter ratio R is between 2 and 20 [20]. This approximation does not take into account the finite length of the rod. The value of effective permeability approaches 0.7 μ_e as the rod becomes fully wound [14].

2.3 Capacitances

Most of the capacitance in the circuit is due to the parallel capacitor. The coil itself has a small capacitance between individual turns [18]:

$$C_t = \frac{\pi^2 2 r_c \epsilon_0 \epsilon_r}{\cosh^{-1}\left(\frac{2r_w + d_w}{2r_w}\right)}, \tag{8}$$

where d_w is the distance or gap between individual wires and ϵ_r relative permittivity of the medium which in a tightly wound coil is the coating on the metal wire. The total capacitance between all turns is

$$C_c = \frac{C_t}{N-1}. \tag{9}$$

2.4 Resistances

The resistances in the antenna are divided into ohmic losses and the radiation resistance. Ohmic losses in the antenna are caused by losses in the wire itself and losses in the ferrite core. Increased losses lead to the antenna being less sensitive at the resonant frequency. The half-power bandwidth also becomes wider.

2.4.1 Skin effect loss

The skin effect is caused by eddy currents in the conductor. A current flowing in a conductor creates a magnetic field around it. Magnetic field induces circular eddy currents that oppose the change in the magnetic field. This leads to the eddy currents being in the opposite direction of the original current flow in the center of the conductor. Near the surface or skin of the conductor the eddy currents flow in the original current direction. Most of the current now flows near the conductor surface thus the effective conducting area is reduced. [21] The skin depth of a good conductor (depth where the current is $1/e$ of the surface current) is given [22, p. 20] by

$$\delta = \sqrt{\frac{2}{\omega \mu \sigma}} \tag{10}$$

The surface resistance of a conductor is [14]

$$R_s = \sqrt{\frac{\omega \mu}{2\sigma}} \tag{11}$$

For a wire with length l_w and radius r_w the wire resistance is [14]

$$R_w = \frac{l_w}{2\pi r_w} \sqrt{\frac{\omega \mu}{2\sigma}} \tag{12}$$

For a coil with a radius r_c this becomes [14]

$$R_w = N \frac{r_c}{r_w} \sqrt{\frac{\omega \mu}{2\sigma}} \tag{13}$$

2.4.2 Proximity effect loss

The proximity effect loss is similarly to the skin effect caused by eddy currents. The magnetic field created by a conductor induces eddy currents in nearby conductors. [21] The magnitude of promixity effect loss is difficult to determine and analytical solutions for proximity effect calculation are complicated but generally the effect is more prominent with larger and more tightly wound coils. It is also dependent on the conductor radius itself. Skin effect and promixity effect can be added together in the wire resistance equation as

$$R_w = N\frac{r_c}{r_w}\sqrt{\frac{\omega\mu}{2\sigma}}\left(\frac{R_p}{R_0}+1\right), \tag{14}$$

where the ratio R_p/R_0 is a factor of how much the total wire resistance is increased due to the proximity effect [23]. By knowing the easily calculated skin effect resistance, the proximity effect can be determined with other means such as simulations and measurements. One method to calculate proximity effect losses is given in [18].

2.4.3 Ferrite core loss

Ferrite core is a lossy material that absorbs power from the magnetic field flowing through the coil. The magnitude of the ferrite loss depends on the material of the rod and the dimensions of both the wire coil and the rod. The equation for the ferrite loss is [18]

$$R_f = \omega\mu_0\mu_e \tan\delta_m N^2 \frac{A}{l_f}, \tag{15}$$

where $\tan\delta_m$ is the magnetic loss tangent or the ratio of imaginary and real components of permeability. Ferrite core losses end up being the main contributing factor to the total ohmic losses in many practical ferrite rod antennas.

2.4.4 Radiation resistance

Radiation resistance is the portion of power in the antenna that is not converted into heat as an ohmic loss. Ferrite rod antenna's radiation resistance is [14]

$$R_r = 31200\left(\frac{\mu_e N A}{\lambda^2}\right)^2, \tag{16}$$

where λ is the wavelength. The factors that determine the radiation resistance also affect the ferrite losses given by equation (15). By choosing a ferrite material with low losses the net effect is positive regarding antenna's receiving performance.

2.4.5 Capacitor losses

Real capacitors have non-idealities from the packaging of the component. These include parasitic capacitance and inductance and series resistance. [24] Typically the quality factor of a capacitor is very high so the resistive losses tend to be very small and negligible [24]. In voltage controlled varactor diodes the series junction

and contact resistance is typically only a few ohms [22, p. 537], which is very small compared to ferrite core and coil losses in equations (15) and (14).

2.5 Quality factor

Quality factor of a resonator, Q, indicates its bandwidth relative to the center frequency [22]:

$$Q = \frac{f}{\Delta f} \tag{17}$$

Alternatively it can be defined as a ratio of average stored energy and energy loss:

$$Q = \omega \frac{W_m + W_e}{P_{loss}}, \tag{18}$$

where W_m and W_e are the average magnetic and electric energy stored in the circuit and P_{loss} is the power loss [22, p. 274]. At resonance W_m and W_e are equal. As the ferrite rod antenna is not a pure parallel resonator mainly due to the series resistance of the inductor, the quality factor is derived from the total quality factor of the individual quality factors of the inductor and the parallel capacitor:

$$Q_i = \frac{\omega L}{R_i} \tag{19}$$

$$Q_c = \frac{1}{\omega C R_c} \tag{20}$$

The resulting quality factor is [22]

$$\frac{1}{Q} = \frac{1}{Q_i} + \frac{1}{Q_c} \tag{21}$$

$$\Rightarrow Q = \frac{\omega L}{\omega^2 L C R_c + R_i} \tag{22}$$

which at resonance becomes

$$Q = \frac{\omega L}{R_c + R_i} \tag{23}$$

Typically capacitors have a much higher quality factor with a small resistance R_C compared to the coil resistances. The quality factor of the system is determined by the quality factor of the coil.

2.6 Induced voltage from an electromagnetic field

The incident electromagnetic field that induces the voltage in the coil can be modeled as a voltage source in series with the coil as shown in figure 4.

The antenna is a loop antenna so it is sensitive to the magnetic field. The electromotive force induced the coil is due to a changing magnetic flux according to Faraday's law:

$$U_{coil} = -N \frac{d\Phi}{dt}, \tag{24}$$

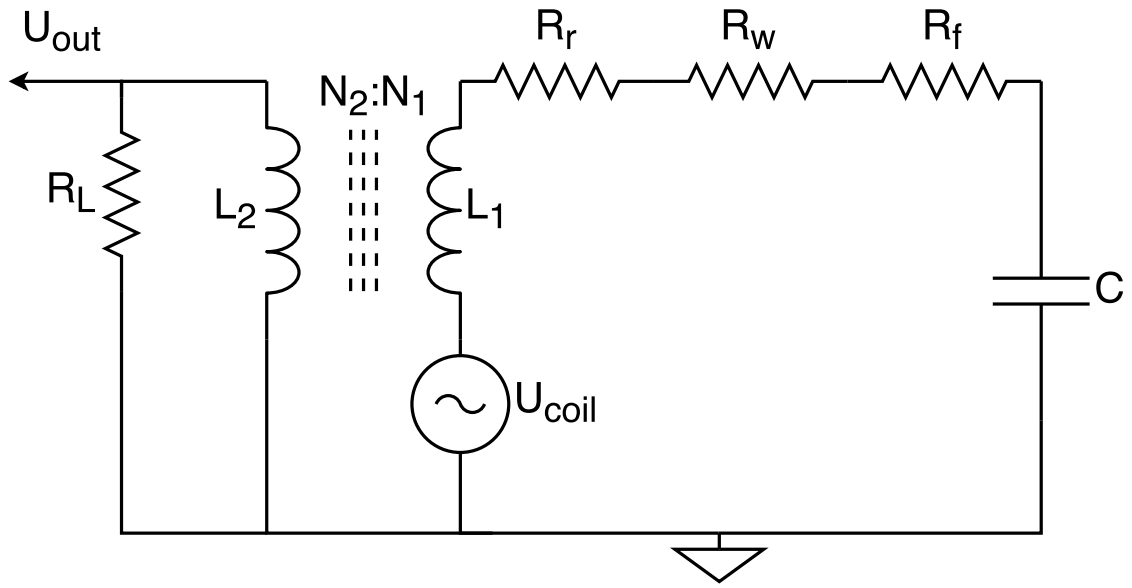

Figure 4: Equivalent antenna circuit for an external field inducing voltage in the coil. The capacitance between coil turns is not shown.

where the magnetic flux is defined as the total flux density over a surface, as

$$\Phi = \iint_S \mathbf{B} dS. \tag{25}$$

If we consider a sinusoidal magnetic field

$$B = B_0 \sin \omega t = \mu_r \mu_0 H_0 \sin \omega t \tag{26}$$

that is parallel to the coil axis, the induced EMF in the coil is

$$U_{coil} = -\mu_r \mu_0 \omega H_0 A N \cos \omega t \tag{27}$$

The induced voltage is proportional to the frequency f. When the coil is part of a resonance circuit the induced voltage is

$$U_1 = U_{coil} \frac{Z_C}{Z_L + Z_C} = \frac{U_{coil}}{j\omega[R_w + R_f + R_r]C - \omega^2 LC + 1}, \tag{28}$$

where Z_C is the impedance of the parallel capacitance and Z_L is the impedance of the coil. At the resonance frequency the above equation simplifies to $U_1 = U_{coil}Q$. The quality factor, which is dominated by the coil ohmic losses, not only affects the bandwidth but also the voltage induced in the resonance circuit.

2.7 Pick-up coil

The impedance in the antenna's main RLC circuit is not well matched to 50 Ω. The induced voltage is highly reflected if connected directly to a 50 Ω input. One way to

improve the matching is to use a secondary coil or a so called pick-up coil next to the main coil. The pick-up coil will act as an impedance transformer. The impedance transformer transforms the main coil impedance and voltage into the secondary coil according to the equation [25]

$$\frac{N_2}{N_1} = \frac{U_2}{U_1} = \sqrt{\frac{Z_2}{Z_1}}. \tag{29}$$

When the pick-up works as intended the output voltage from the decreased secondary coil voltage is still higher than the original main coil output voltage due to the improved matching.

When inductors are coupled a current change in one inductor induces a voltage in the second inductor. The mutual inductance between the inductors is defined as [25]

$$M = k\sqrt{L_1 L_2}, \tag{30}$$

where k is the coupling coefficient. The equivalent circuit of two coupled inductors is a T-circuit shown in figure 5.

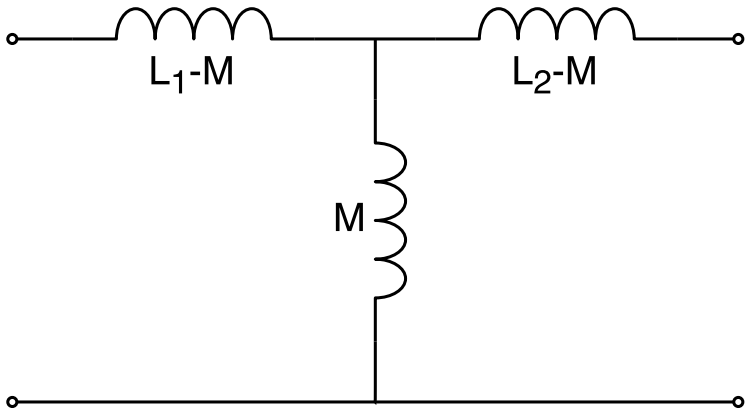

Figure 5: Equivalent circuit of two coupled inductors.

The voltage over the two coils can be expressed with the mutual inductance as the following:

$$U_1 = j\omega \left(L_1 I_1 + M I_2\right) \tag{31}$$
$$U_2 = j\omega \left(M_1 I_1 + L_2 I_2\right), \tag{32}$$

The coupling coefficient of the two coils can be measured by changing the secondary coil from open circuit to shorted and observing the change in the resonant frequency. When the second coil is shorted the voltage in the secondary coil becomes zero and the current will be

$$I_2 = -\frac{M I_1}{L_2} \tag{33}$$

By inserting this into the voltage equation of the primary coil in equation (32):

$$U_1 = j\omega \left(L_1 I_1 - \frac{M^2 I_1}{L_2} \right) \tag{34}$$

$$= j\omega \left(L_1 - \frac{M^2}{L_2} \right) I_1 \tag{35}$$

$$= j\omega L_s I_1, \tag{36}$$

where L_s is the apparent/measured inductance over the primary coil when the secondary coil is shorted. Now the mutual inductance squared can be written as

$$M^2 = L_2 \left(L_1 - L_s \right) \tag{37}$$

Using this the coupling coefficient becomes

$$k = \frac{M}{\sqrt{L_1 L_2}} = \sqrt{1 - \frac{L_s}{L_1}} = \sqrt{1 - \left(\frac{f_o}{f_s} \right)^2}, \tag{38}$$

where f_o and f_s are the resonance frequencies related to the inductances L_1 and L_s according to equation (2) with the secondary coil open and shorted, respectively.

The impedance at the antenna output is Z_2. A portion of the pick-up voltage U_2 is reflected at the antenna output according to equation [22]

$$\Gamma = \frac{Z_L - Z_2}{Z_L + Z_2}, \tag{39}$$

where the load impedance is 50 Ω. The output voltage of the antenna is

$$U_{out} = (1 - \Gamma) U_2. \tag{40}$$

2.8 Antenna effective height

Effective height of an antenna is one way to measure antenna's operation. It is defined as the ratio of induced voltage at the output port, U_{out}, and incident (electric) field E, as

$$h_e = \frac{U_{out}}{E} = \frac{1}{\mu_0 c_0} \frac{U_{out}}{H} \tag{41}$$

This kind of measure takes into account the quality factor of the RLC circuit, the impedance and voltage transformation from the pick-up coil and the reflection at the output port. The induced voltage in the coil might be higher for a certain antenna but due to the aforementioned reasons the real measurable parameter which is the output voltage might be in fact lower. The effective height makes comparison of different antennas simple.

2.9 Antenna polarization

Ferrite rod antenna is so called linearly polarized antenna. A linearly polarized antenna is capable of receiving both linear and elliptical polarization including circular polarization. In worst case scenario the incident electromagnetic radiation has a polarization perpendicular to the antenna's polarization and theoretically nothing is received. A wave at 45 degree angle of polarization half of the incident power is lost.

2.10 Antenna directivity and efficiency

Antenna directivity (denoted with D) means how much more power is directed in the main direction of the antenna compared to an isotropical radiator. An isotropical radiator/antenna is a theoretical concept that cannot be realized but is useful in antenna theory nevertheless. All incident power is radiated from the isotropical antenna in a uniform fashion.

The radiation efficiency of an antenna is defined as the portion of power that is not absorbed in the antenna structure as ohmic losses. This is characterized by the radiation resistance, R_r, and the ohmic loss resistance, R_{loss}, with which the radiation efficiency, η_r, is

$$\eta_r = \frac{R_r}{R_r + R_{loss}} = \frac{P_{rad}}{P_{in}} = \frac{P_{rad}}{P_{rad} + P_{loss}}, \tag{42}$$

where P_{rad} is the radiated power, P_{in} is the power accepted by the antenna and P_{loss} is the power loss in the antenna. The antenna has losses due to the impedance mismatch between the antenna output and feed input. The mismatch causes power reflection. The total efficiency of the antenna is defined as [26]

$$\eta_t = (1 - |\Gamma|^2)\eta_r, \tag{43}$$

where Γ was defined in equation (39). These are used to define antenna gain, G, and realized gain, G_{real}, respectively:

$$G = \eta_r D \tag{44}$$

$$G_{real} = \eta_t D. \tag{45}$$

2.11 Radiation pattern

Radiation pattern of an antenna gives the directional information how the radiated power of the antenna is distributed or how effectively it receives radiation from certain directions. Antennas can have a highly directive radiation pattern with a narrow main-lobe. In addition to the main-lobe an antenna often has multiple undesirable side-lobes that are defined by their direction and power relative to the main-lobe (side-lobe level, SLL).

Ferrite rod antenna has an omnidirectional radiation pattern similar to a small loop antenna as illustrated in figure 6. The radiation pattern is also the same as for

a small dipole antenna. The nulls in the radiation pattern are located in the coil axis (marked as the z-axis in the figure 6). An often used parameter for radiation pattern is its half-power beamwidth (HP) which means the angle from which the received power is at least half of the maximum. For small loop antennas this angle is 90 degrees.

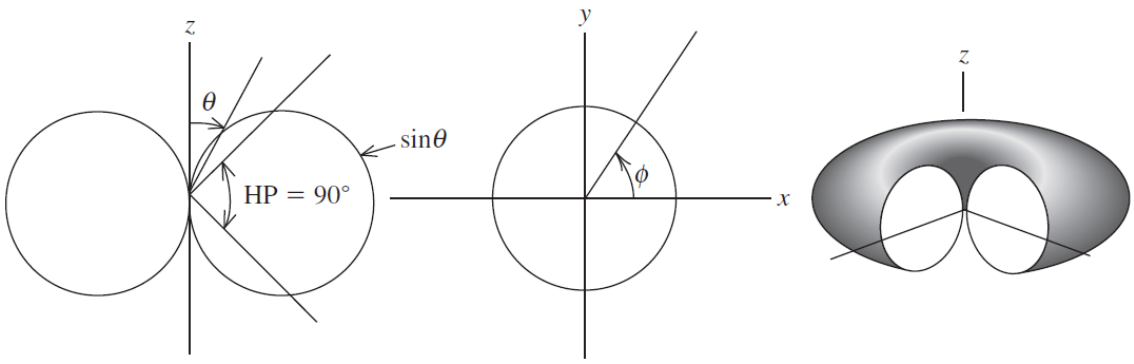

Figure 6: Radiation pattern of small loop antennas in spherical coordinates [14, p. 37]. The $\sin\theta$ pattern (left figure) is omnidirectional for all azimuthal angles ϕ (middle figure) resulting in a torus shaped pattern in three dimensions (right figure).

The omnidirectional radiation pattern means that the antenna is able to receive signals from multiple directions. This is useful when signal sources and their directions are unknown or difficult to predict. The directional information is mostly lost but ray tracing, analyzing the Poynting vector path associated with the electromagnetic wave, can be used to estimate the signal origin.

2.12 AM modulation

Amplitude modulation utilizes a radio frequency carrier signal that is modulated with a signal containing the information such as speech or music. The output signal is generated using heterodyne technique where the carrier signal is generated in a local oscillator and combined with the information signal in a mixer. [25] Figure 7 shows the main blocks of a superheterodyne receiver. The radio frequency signal from the antenna, f_{RF}, is amplified in an RF amplifier. The amplified signal is mixed down to intermediate frequencies, f_{IF}, by using a local oscillator operating at frequency f_{LO}. The intermediate frequency is then filtered in a band-pass filter, amplified again and finally demodulated.

A transmitted output signal consists of the carrier signal at the center frequency and the information signal as two sidebands around the center frequency. The total bandwidth taken by a typical AM broadcast is approximately 10 kHz. The actual signal level is also dependent on the modulation index.

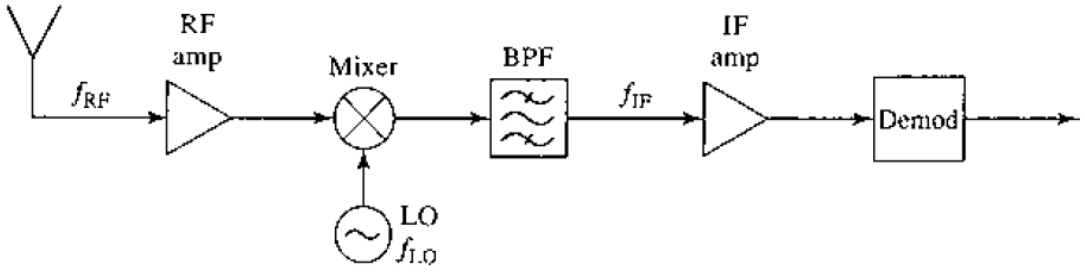

Figure 7: Block diagram of a superheterodyne receiver. [22, p. 673]

2.13 Radiowave propagation

Generally speaking, radiowaves emitted from a transmitter are propagated to all directions in a spherical manner. At distance r the power density of the wave, S, is [14, p. 109]

$$S = P_t G_t \frac{1}{4\pi r^2}, \tag{46}$$

where P_t is the transmitted power and G_t gain towards a specific direction. The power density can be used to express the electric and magnetic field with the impedance of free space ($Z_0 \approx 376.73\ \Omega$) as

$$Z_0 = \frac{E}{H} = \frac{E^2}{S} = \frac{S}{H^2}. \tag{47}$$

The relationship between transmitter output power and receiver input power is the Friis transmission equation [14, p. 109]:

$$\frac{P_r}{P_t} = G_r G_t \left(\frac{\lambda}{4\pi r}\right)^2, \tag{48}$$

where the free-space path loss is

$$L_{fs} = \left(\frac{4\pi r}{\lambda}\right)^2. \tag{49}$$

As the free-space path loss is proportional to the square of the propagation distance the power of the wave attenuates 20 dB as the distance increases tenfold.

In reality the radiowave behavior in medium and high frequencies is depends on the ionospheric conditions. The waves can fully refract and bounce between the ionosphere and Earth before penetrating the ionosphere thus increasing the propagation distance and losses. Due to Earth's magnetic field and the ionospheric plasma the wave separates into two different modes: the ordinary mode (the O mode) and the extraordinary mode (the X mode). They can have drastically different propagation paths and the receiver of a signal might actually only receive one of the modes which has less power than the original wave would have had. [27]

2.13.1 Ray tracing

Ray tracing is a technique where the path of the wave is obtained by following the direction of the Poynting vector. The method can be used to determine the origin of the signal source for complex non-direct signal paths and with no knowledge of the direction of the received signal. The received signal from the antenna will have a certain frequency, bandwidth, modulation, signal strength and the timestamp when the signal was received. These can be compared to radio broadcasting catalogs listing all radio broadcasts and their transmitter locations on Earth.

Ionospheric models can be used to construct a ray tracing program that calculates the path of radio waves. From a certain location on Earth the rays will propagation in a spherical fashion until the ionosphere starts to affect the rays. Depending on multiple factors such as frequency, ray direction, direction of the background magnetic field, and the ionospheric properties the rays will take different paths. Some ray paths might eventually penetrate the ionosphere. If such ray intersects with the satellite it might be the origin of the received signal.

With enough computer power and smart algorithms a matching ray from a suitable candidate station to the satellite can be found. A faster and less intensive method is to use the satellite as the origin of the rays and observe in which locations on Earth they are traced. Although the propagation path through ionosphere is not exactly reversible in many cases it is approximately good enough to locate the general area of the ray's origin in the frequency region of 1 – 6 MHz analyzed on this work (see e.g. [28] for discussions about the reversibility in the Earth's ionosphere).

2.14 Environment in space and during the launch

Launch is a very critical part of the mission in terms of failure rate. The launch rocket itself can fail or the satellite or parts of it might start to vibrate destructively during the launch. During the launch the satellite and the antenna will experience high levels of vibration originating from both structural vibration and noise field, high acceleration during ascent and mechanical shock [5, p. 12]. In the design of the final radio instrument featuring ferrite rod antennas these need to be taken into account to minimize the risk of instrumentation failure.

The vacuum of space and other phenomena on the orbit differ from the typical antenna and radio use. In satellite all components and instruments have to be made of low-outgassing materials. Materials that have a high outgassing rate in vacuum pose a problem to many systems in the satellite, for example, the outgassed molecules might obstruct camera instruments or solar panels. [5, p. 583]

The antenna itself is made a ceramic nickel-zinc ferrite. The coil wire is made of copper. The wire has a thin layer of insulating material which can be made of polymer film. The insulating material specifically should be chosen to have low outgassing rate. The removal of the coating will create a direct connection between adjacent windings in the coil severely affecting the operation of the antenna and ultimately causing it to fail.

In addition to sublimitation the coating can suffer material damage from exposure

to UV radiation which can modify the chemical bonding structure of the material [5, p. 42] with the same effect as outgassing. In general the antenna and the radio should be protected from outside energetic radiation. The most critical components to antenna's operation are semiconductor tuning capacitors.

External heat input to the satellite consists of three sources: the Sun, Earth's albedo and Earth's infrared radiation [5]. The amount of heat input varies for different orbit altitudes and during the day-night cycle. Suomi 100 satellite temperature variation can be said to be from -50 °C to 50 °C. Inside the satellite the temperature stays relatively constant. The temperature variations will cause thermal expansion in the antenna and its materials and also change the relative permeability of the ferrite.

Interference from the satellite systems needs to be taken into account. All electric circuitry produces noise that the antenna or the radio circuitry might pick up. The local interference originating from electrical devices has a strong electric near-field and a weak magnetic field. Antenna should be shielded from the inner parts of the satellite in a way that it does not affect the performance.

2.14.1 Antenna calibration while deployed

When deployed the antenna's operation is affected by multiple factors. These include the temperature variations in space. Ferrite permeability is a function of temperature meaning that the resonance frequency is temperature dependent. The satellite will feature multiple temperature sensors. These can be used to estimate the temperature of the ferrite rod. The effects of the temperature variation on the antenna can be weakened by manufacturing a cover from non-conductive material so that the antenna is not directly exposed to the outside. The temperature dependence of the ferrite material is known [19] and can be taken into account in the radio control software.

Known signals such as emissions from EISCAT can be used to determine what is the actual resonance frequency of the antenna. The antenna and the radio receiver are tuned to the same frequency but antenna might actually resonate at a slightly different frequency. By having a known source and frequency this offset is found and the antenna and data can be calibrated.

3 Research material and methods

3.1 Ferrites

Ferrite materials come in a wide range of properties suitable for variety of different applications. Ferrites are ceramic compounds and they are divided into soft and hard ferrites based on their coercivity. Soft ferrites with low coercivity are used in ferrite rod antennas. They are commonly made of either manganese-zinc or nickel-zinc combined with iron oxides. Two main factors when choosing the material are low losses and stability over the frequency range of the antenna. Fair-Rite is a company that manufactures many different types of ferrite cores [19]. Four ferrite materials that Fair-Rite manufactures as rods and are suitable for low frequency inductive applications are listed in table 2. Loss factor is a unitless ratio $\tan\delta_m/\mu_r$.

Table 2: Fair-Rite ferrite materials for low frequency antennas.

Material	**Frequency range**	μ_r	**Loss factor**
33 (MnZn)	$<$ 3.0 MHz	600	25×10^6 at 0.2 MHz
61 (NiZn)	0.2 – 5 MHz	125	30×10^6 at 1 MHz
67 (NiZn)	$>$ 0.5 MHz	40	150×10^6 at 50 MHz
78 (MnZn)	$<$ 200 kHz	2300	4.5×10^6 at 0.1 MHz

Overall the best performance is given by material numer 61 (NiZn), which combines low losses and a frequency range matching the requirements. It is suitable for inductive applications even up to 25 MHz [19, p. 9]. Rods made of this material are also sold by other companies such as Amidon [29].

3.1.1 Modified inductance formula

Fair-Rite catalog has charts from which to calculate the inductance [19]. Initial testing with different coils showed that these give a more accurate inductance than equation (5). Based on these charts an equation to fit the data can be formed. The better approximation for the effective permeability of material number 61 ($\mu_r = 125$) can be written as

$$\mu_e = 2.625 R_{LD}^{1.131} \left(8.141 - 7.096 \left(\frac{2 r_w N}{l_f} \right)^{0.1291} \right), \tag{50}$$

which also takes into account the size of the coil ($2r_wN$) relative to the core length (l_f). Figure 8 shows how the modified inductance formula gives a good correspondence to the data provided by Fair-Rite up to length-to-diameter ratios R_{LD} of 10.

3.2 Variable capacitors

Variable capacitors also known as varactors can be used as a tunable capacictance in an RLC circuit. A reversed-biased p-n junction has a voltage-dependent capacitance.

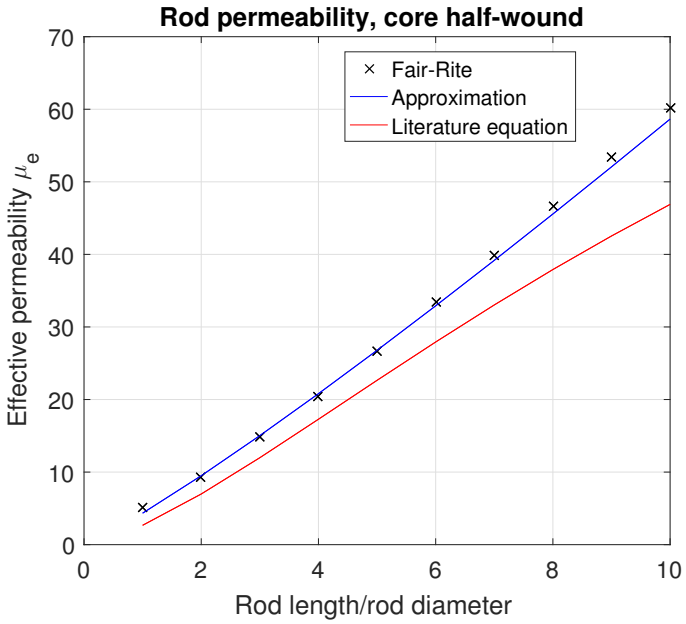

Figure 8: Calculated effective permeability. Black crosses are permeability values determined from Fair-Rite charts of which the blue line (equation (50)) is an approximation. Red line is calculated with equation (6).

Higher bias voltage widens the depletion zone in the junction leading to a lower capacitance. The capacitance profile of a reversed-biased p-n junction follows the equation [22, p. 537]

$$C(U) = \frac{C_0}{(1 + U/U_0)^n}. \tag{51}$$

The junction doping profile exponent n is 0.47 for many varactors but can be as high as 1.5 or 2.0 [22]. The resonance frequency in equation (2) depends on the capacitance as $C^{-0.5}$. The frequency tuning of the antenna becomes linearly dependent on voltage if varactors with a doping profile n = 2.0 are used. A higher exponent leads to a larger capacitance range.

Varactors manufactured by Skyworks in SMV1247-SMV1255 series [30] have properties that make them suitable for antenna tuning capacitors. They have a high capacitance ratio meaning single varactor can be used to tune to a wide range of frequencies. They also have a low tuning voltage which is ideal for the nanosatellite. The operating temperature range covers the temperature variations expected on orbit.

The widest capacitance range in the acquired varactors is achieved with SMV1253. With a varying voltage from 0 V to 3 V the capacitance in specifications vary from 69.32 pF to 7.77 pF. The middle point in capacitance range is 38.545 pF. [30]

3.2.1 Varactor layout

Varactors are placed in a configuration shown in figure 9 in parallel with the main antenna coil. A single varactor is sufficient to provide the tuning capacitance for the coil. The issue is that a strong enough induced voltage in the coil will also bias the varactor and detune the antenna. Also the DC voltage has a direct connection to the ground through the coil. This is solved by first putting another varactor in series with the first one in opposite direction. This will provide frequency stability as the total capacitance stays relatively constant.

The two varactors are now in series which means that their total capacitance is only half of one varactor. Two additional varactors are required in parallel to the other two to bring the total capacitance back to the same as it was with only one varactor.

3.3 Antenna schematic with the radio IC

The antenna is planned to be used with a commercial radio IC (Si4743 by Silicon Laboratories [12]), which is surface-mounted device with both MW and SW support. It comes in a 24-pin 4×4 mm QFN package. Figure 9 illustrates the radio IC and the pin configuration for antenna considerations. The antenna output is connected to the AMI-pin. Apart from the voltage and ground pins most of the pins are connected to the satellite's main computer (i.MX).

The receiver sensitivity is a voltage level at which the radio is able to distinguish and receive the signal. It is defined for a specific signal-to-noise ratio (SNR) or signal-plus-noise-to-noise ratio (SNNR). Si4743 AM receiver sensitivity is typically 25 dBμV (17.8 μV) defined for SNNR 26 dB. The maximum voltage rating for RF input level peak value at AMI-pin is 0.4 V. The radio input is matched to 50 Ω to which the antenna output should be matched as good as possible.

3.4 Expected field strength

AM broadcasts are some of the strongest man-made signals in MF and HF that are also identifiable by their narrow bandwidth. Transmitter powers vary from below 1 kW for small local stations up to over 1 MW. A simple calculation for field strength levels on orbit can be made using equations (46) and (47). This assumes that the only loss comes from the spherical propagation of the waves. The satellite will orbit at an altitude of approximately 500 km. The direct of line sight between a point on Earth and the satellite varies from 500 km (satellite at zenith, 90 degree elevation) to approximately 2600 km (satellite at horizon, 0 degree elevation). The transmitter radiation pattern can be assumed isotropical so the gain is 0 dB. Table 3 lists the electric field strengths for various distances and transmitter powers.

Studies have been conducted on the field strengths of electromagnetic radiation in the general environment [31]. It should be assumed that only the stations with stronger transmit powers are detectable. Commercial ray tracing software such as Proplab-Pro [32] can be used to calculate possible signal paths and strengths.

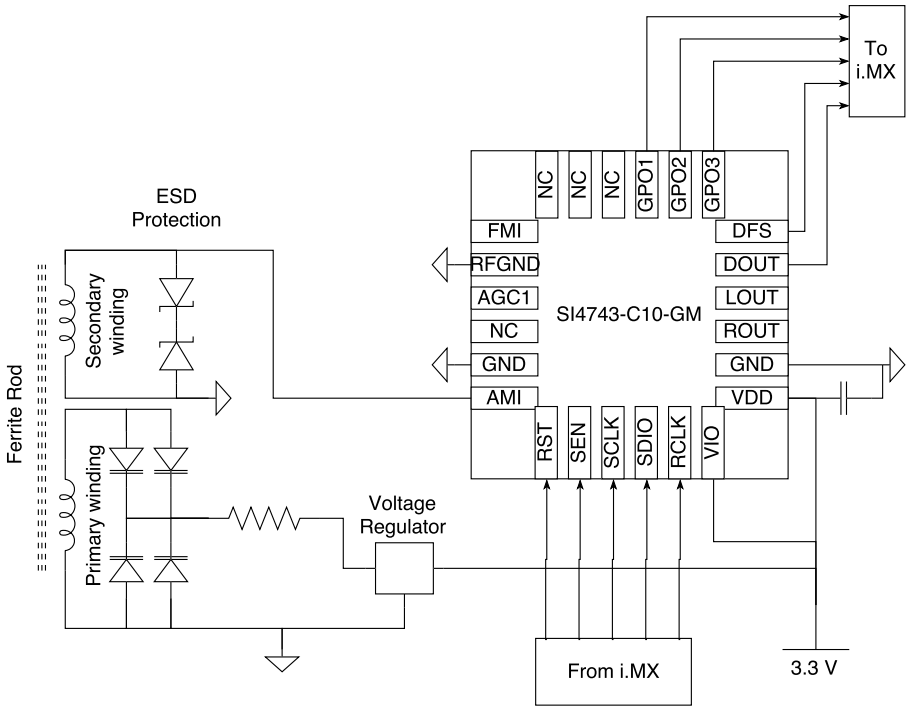

Figure 9: Designed antenna connections to the radio IC used in this work.

Table 3: Electric field strength for various transmit powers and distances.

P_t [kW]	E [mV/m]			
	r = 500 km	r = 1000 km	r = 1500 km	r = 2600 km
1	0.35	0.17	0.11	0.07
10	1.1	0.55	0.37	0.21
100	3.5	1.7	1.2	0.67
1000	11.0	5.5	3.7	2.1

In addition to strong AM broadcasts ionospheric heaters designed to to specifically study the ionosphere can be used. The EISCAT ionospheric heating facility is located in Tromsø, Norway. It has transmitters that are tunable in the frequency range of 3.85 – 8 MHz. The effective radiated power varies with the frequency from 200 MW at 4 MHz up to over 1200 MW at 8 MHz. [33]

3.5 Choosing antennas

In the planned frequency range there are two prominent AM transmission bands at 1.5 MHz and 5.0 MHz. Two of the antennas are designed to have their frequency ranges centered around these frequencies. The third antenna was chosen to be tuned between these two. All three antennas should have partially shared frequency ranges.

In addition is it desirable to cover the widest possible frequency range. From the available ferrite rods and varactors it is possible to iteratively determine the best

combinations of system parameters to get the highest possible voltage output from the antenna. This process is illustrated in figure 10.

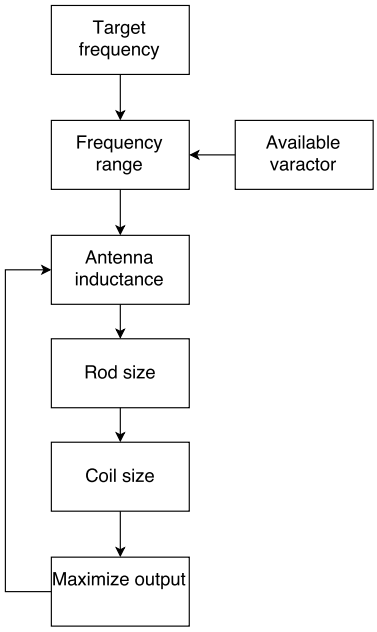

Figure 10: Illustration of the iterative antenna design process used in this work for the Suomi 100 satellite AM radio instrument.

The chosen antennas listed in table 4 all end up using the same rod which is also the largest available that can be integrated to the satellite. With larger rods it's possible to achieve higher effective permeability and Q factor which contribute to the voltage level of the antenna. The minimum and maximum frequencies are determined so that with the available capacitance range the center frequency f_c falls in the middle of the frequency range. The density of the ferrite material used is approximately 4.8 g/cm^3 [19].

Table 4: Antenna parameters.

	Antenna 1 f_c = **1.50 MHz**	Antenna 2 f_c = **3.00 MHz**	Antenna 3 f_c = **5.00 MHz**
Min. frequency (MHz)	0.75	1.51	2.51
Max. frequency (MHz)	2.24	4.51	7.50
Inductance (μH)	650	160	58
Length (mm)	76.2	76.2	76.2
Radius (mm)	9.398	9.398	9.398
N	110	48	26
Mass (g)	27.5	26.3	25.9

3.6 Simulating the antenna

Results and antenna dimensions obtained from theory can be compared against electromagnetic simulations. CST Microwave Studio (CST MWS) is a commercial 3D electromagnetic simulation software by Computer Simulation Software (CST) used for simulating antenna structures. For electrically small devices such as ferrite rod antennas the developer recommends using their frequency domain solver [34] and has illustrated how it can be applied in low frequency antenna simulations [35]. CST provides a workflow documentation to assist in the simulation process [36].

3.6.1 Ferrite material in CST MWS

CST MWS does not provide the used ferrite material in their material list. The important electrical properties can be found from the material's datasheet [19]. In table 5 are listed the parameters used to create a new material in the simulation software. The material parameters stay relatively unchanged over the used frequency range so no frequency dependency was needed.

Table 5: Ferrite material parameters for CST MWS used in the antenna design analysis of this work.

Parameter	Value
Type	Normal
ϵ_r	1
μ_r	125
σ	1e-8 S/m
$\tan\delta_m$	0.038
Thermal type	Normal
Thermal conductivity	4 W/K/m
Heat capacity	0.8 kJ/K/kg
Mechanical type	Normal
Young's modulus	147.1 GPa
Poisson's ratio	0.29
Thermal expansion coefficient	9e-6 1/K
Density	4800 kg/m^3

3.6.2 Simulation accuracy

The simulation environmental parameters for mesh and other accuracies are limited by the physical memory of the computer. It is also beneficial for the design process to be able to get results in relatively short time even though the computer memory would allow longer simulations. The mesh accuracy can be divided into three different parts: the physical antenna and satellite structures, the immediate space surrounding the structures and the space further away extending to the simulation box edges.

To determine how much the mesh accuracy can be reduced without it affecting the results considerably one can simulate simple structures with good accuracy. Then

the accuracy will be decreased gradually and the changes in results are observed. This way a lower boundary for acceptable mesh size can be determined. During the simulation process the accuracy can be increased periodically to see if more complex structures cause more differentiation with lower accuracy settings.

3.6.3 Validating the settings

The order of simulations are done from simple to more complex structures. This way the result deviation from theory can be more accurately located should it happen.

First priority is to confirm that the used solver and other simulation setup parameters produce results that match the theory for the simplest structures. A simple air coil can be simulated for skin and proximity effect and air coil inductance. The proximity effect can be separated from the skin effect by making the coil less tightly wound, effectively making it resemble a straight wire.

After determining skin and proximity effect a ferrite core will be introduced to simulate ferrite losses. Now the three main ohmic losses are found and separated. The inductance of the ferrite rod coil can be compared against the theoretical value.

The aforementioned steps should be repeated for different size rods and coils. In addition to chosen ferrite rod (76.2×9.398 mm) which is one of the largest available rods a smaller rod (35×5 mm) from the lower end should be used.

3.6.4 Single antenna simulations

With the antenna model the actual operation of the antenna can be simulated. The feed network and parallel capacitance can be formed using lumped elements. The antenna forms a two-port network with the main and pickup coil outputs. The main port (labeled as port 1) is in practice an open circuit and should be modeled as a high impedance discrete port. The actual antenna output (port 2, pickup coil) is 50 Ω. The operation of the impedance transformer can be verified by varying the pick-up coil parameters. These are the distance between the two coils and the turn ratio.

Two different types of radiation excitation can be used. Far-field excitation corresponds to the actual situation where the antenna acts as a receiving antenna. The output voltage in port 2 results from the incident electromagnetic field. Port excitation is used to calculate scattering parameters and radiation pattern.

3.6.5 Multiple antenna simulations

The same simulations for multiple antennas can be done as for a single antenna. The additional information gained is their mutual coupling and effect on each other when the space for antennas is limited.

Scattering parameters are used to describe an electrical network. An electrical network can be defined as having N-ports. Each S-parameter is associated with two ports and describes the power flow from one port to other ports. Two antennas in close proximity cause interference to each other. The effect can be evaluated by using

scattering parameters for a 4-port network, as

$$\mathbf{S} = \begin{bmatrix} S_{11} & S_{12} & S_{13} & S_{14} \\ S_{21} & S_{22} & S_{23} & S_{24} \\ S_{31} & S_{32} & S_{33} & S_{34} \\ S_{41} & S_{42} & S_{43} & S_{44} \end{bmatrix}, \tag{52}$$

where for S_{xy}, x is the output port and y the input port. [14] [22] Altenatively a simple voltage measurement from the antenna output port can show how much the signal level changes compared to when the antenna is simulated in free-space.

Testing mutual coupling should be done in two different main configurations: first a case where the axis of both antennas is in parallel with the incident magnetic field lines, and second a case where one antenna is perpendicular to the other antenna and the magnetic field lines. Additionally for both cases there are different possible configurations for the main and pickup coils. All these variations are shown in the figure 11.

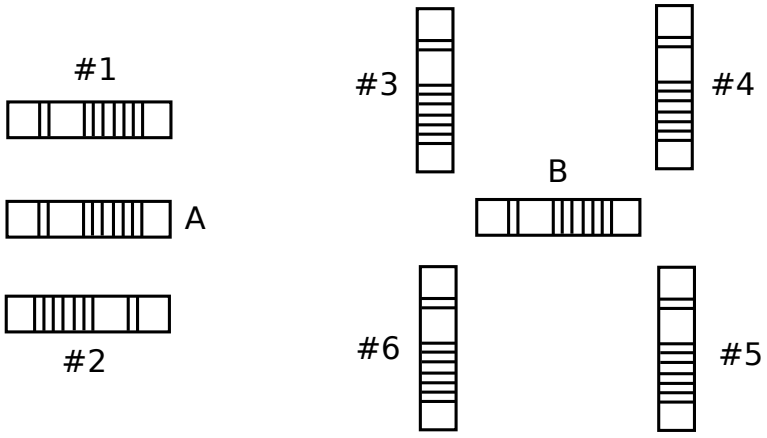

Figure 11: Different coil configurations. The ferrite rod antennas marked A and B are the reference antennas. A second antenna is rotated and moved around them to six different positions (marked as antennas 1 – 6).

3.6.6 The satellite model

The satellite model uses the main conductor elements in the satellite: the body of the satellite, the camera and the UHF PCB. The satellite body is made of aluminium. All large features with electrical properties should be modeled but for reduced simulation time finer details can be left out from the model. This is easily manageable in the software where you can choose which modeled components are used.

In addition to the satellite model a hollow rectangular metallic tube with open ends was modeled. This corresponds to measurements made with a similar object having the same outer dimensions as the satellite. The purpose is to observer whether simulations are predict real measurements accurately or not.

3.6.7 Antenna operation with the satellite body

The last step in simulations is to introduce the satellite model and conduct same simulations as were done before. The satellite sets limitations to antenna positioning. By simulating realistic antenna positions and comparing the results to the reference level where there is no interfering satellite body the frequency detune and attenuation levels can be determined.

There are three alternative places for antennas (figure 12). They can either be placed in the free space at the satellite's either end. It is also possible to develop an extension mechanism that is triggered when the satellite reaches the orbit. The antennas are then extended up to 4 cm off the satellite's sides.

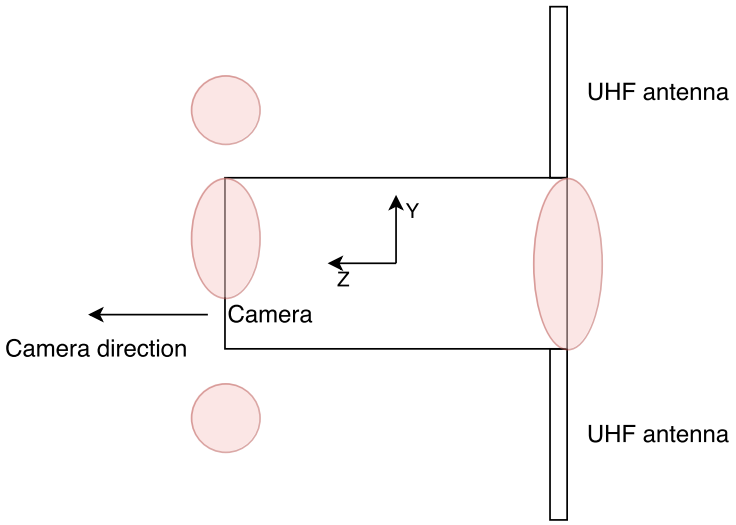

Figure 12: Illustration of general areas where the antennas can be placed which are marked in the figure. The origin is at the center of the satellite.

3.7 Testing a prototype

The described RLC circuit can be tested by constructing a prototype antenna consisting of the ferrite rod, main and pick-up coils and the parallel capacitor. The circuit performance can be tested by using a signal generator to simulate the electromagnetic field.

Simply measuring how the circuit operates internally is not enough to fully understand how the antenna works with a real field. A typical way to measure antenna's receiving/transmitting performance is to use an anechoic chamber. An alternative to this is a gigahertz transverse electromagnetic (GTEM) cell [13].

3.7.1 Measurements with a GTEM cell

A GTEM cell is an electromagnetic compatibility test chamber illustrated in figure 13. It is a hollow metal structure that has a 50 Ω input and load that are connected with

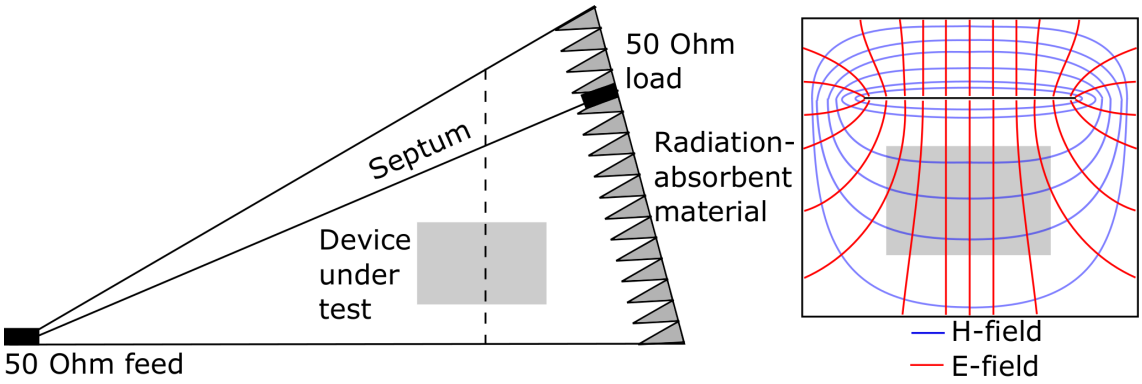

Figure 13: Illustration of a GTEM cell used in the antenna test in this work.

a stripline conductor known as septum. Additionally the back wall has radiation-absorbent material. The cell creates a TEM wave inside it. Inside a designated test area, where the device under test is placed, the field lines point in the same directions over the whole area. This means that the DUT effectively sees an incident plane wave radiation. The GTEM cell used in the measurements had a test area of 23 x 17 x 10 cm [37]. The 2.2 meter long cell is shown in figure 14.

There are some advantages of a GTEM cell measurement over using an anechoic chamber. True far-field conditions can't be achieved in an anechoic chamber for a low frequency antenna. As the GTEM cell is a radiator itself no additional transmitter antenna is needed [13]. Such an antenna would have to built and tested before using it. GTEM cell also requires less power and amplification to generate a desired field strength compared to an anechoic chamber [13].

The field strength can be calculated from a simple equation [37]

$$E = \frac{U}{h} = \frac{\sqrt{PZ}}{h}, \tag{53}$$

where P is the input power fed into the GTEM feedpoint, Z is the input impedance of the cell (50 Ω) and h is the height between the septum and the chassis at the DUT.

Antenna receiving properties can be tested with the following equipment:

- GTEM cell
- signal generator
- power meter
- voltage/power measurement device (e.g. an oscilloscope)
- coaxial cables

The test setup is illustrated in figure 15. The signal generator is connected to the feedpoint of the GTEM cell (with an input impedance Z) and a power meter, which

Figure 14: GTEM cell at Aalto University, Otakaari 5A, which was used in the measurements with the side panel removed. Photo taken by Petri Koskimaa.

measures the input power P. The antenna (DUT) is then placed inside the cell through the door on the side of the cell where the septum-to-floor height is h. The resulting field strength at a frequency f can then be determined from equation (53). The output port of the antenna is connected to a voltage measuring device such as an oscilloscope. The measured output U_{out} corresponds to voltage in equation (40).

These measurements can be repeated with a metallic satellite body to measure the effect it has on the antenna performance. Another common measurement device in RF measurements is a network analyzer, which is used to get the network parameters of the device.

3.7.2 Error sources in measurements

Due to the prototype nature there are many factors that can produce errors in the measurements. The coils of the antenna were hand-wound with overlapping windings and not a uniformly tight finish. This can have an effect on the inductance of the antenna.

The test board used had parallel connectors rows with metallic sheets connecting the individual connectors within the rows. Parallel metallic sheets act as an capacitor

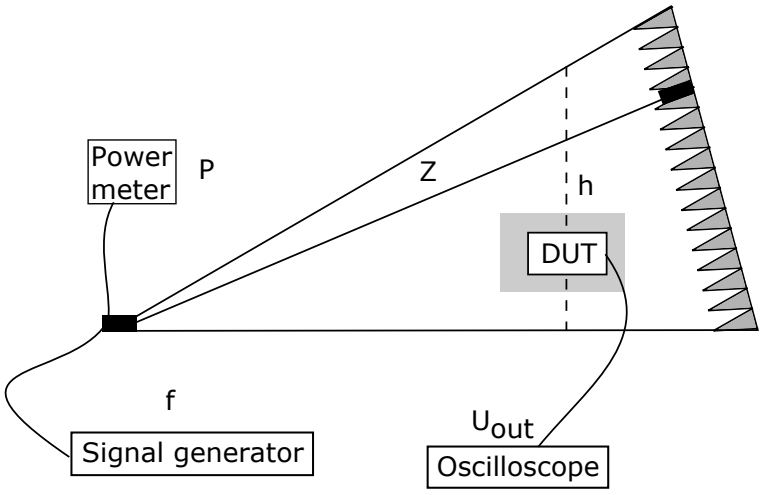

Figure 15: Test setup used in the GTEM measurements.

which introduces parasitic capacitances in the circuit.

Antenna displacement inside the GTEM cell was unavoidable due to the small working space inside the cell. The antenna was positioned and turned by hand instead of a mechanical system. Much care was nevertheless taken in getting a high accuracy.

GTEM cells and the used GTEM cell in particular have specified test areas where the device is placed [37]. Conducting material such as the satellite body or cables outside this area can affect the test results. Such situations arose when the antenna needed to be away from the metallic body or when the metallic body was rotated along with the antenna.

Full exhaustive tests for the GTEM cell were not conducted. Previously done testing for the cell in question was used instead. Dynamic range of the GTEM cell used is 20 dB. The original tests made after the cell was built went only as low as 10 MHz. [37].

4 Results

4.1 Simulations

The simulations were conducted in three different phases. First the simulation setup was confirmed by obtaining RLC parameters from simple air-filled coils. Then the same simulation was done to a ferrite rod antenna. After comparing the parameters to theoretical values and finding that they are in agreement the satellite body was added to the simulation. First a simple structure with only the outer edges of the satellite aluminium body was used. Finally a more accurate model of the satellite was used.

The ferrite rod and the coils were modeled as shown in figure 16. Due to simulation technicalities caused by the tetrahedral mesh formation there is a tiny gap between the ferrite rod and the coil. Likewise the coil windings have a small separation between each other. Real copper wire also has a very thin layer of coating of insulating material which is effectively the same what was modeled here.

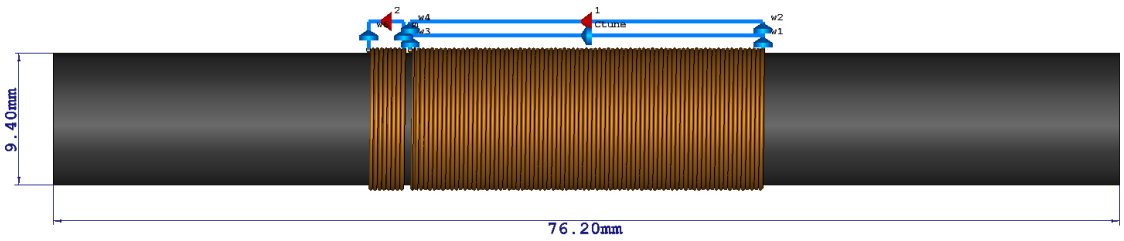

Figure 16: An example model of the ferrite rod antenna in CST MWS featuring two coils (80 turns in the primary winding and 8 in the secondary winding), two ports and lumped element networks.

In the simulation file the satellite body was modeled according to the specifications that were discussed with professor Esa Kallio. The modeled parts (shown in figure 17) were the satellite body itself, camera compartment made of aluminium, UHF antenna PCB and supporting structures related to the launch. Also shown in the figure are three ferrite rod antennas that are placed in the location above the camera compartment corresponding to the location shown in figure 12.

4.1.1 Skin and proximity effect

The proximity effect is caused by parallel wires in close proximity. An air-filled coil was simulated to study proximity effect by increasing the distance between individual windings by changing the coefficient K which determined the coil length as

$$l_c = K2r_wN. \tag{54}$$

As the winding separation increases the coil start to resemble a straight wire which would have zero resistance caused by the proximity effect. The simulated structure parameters and results are shown in table 6.

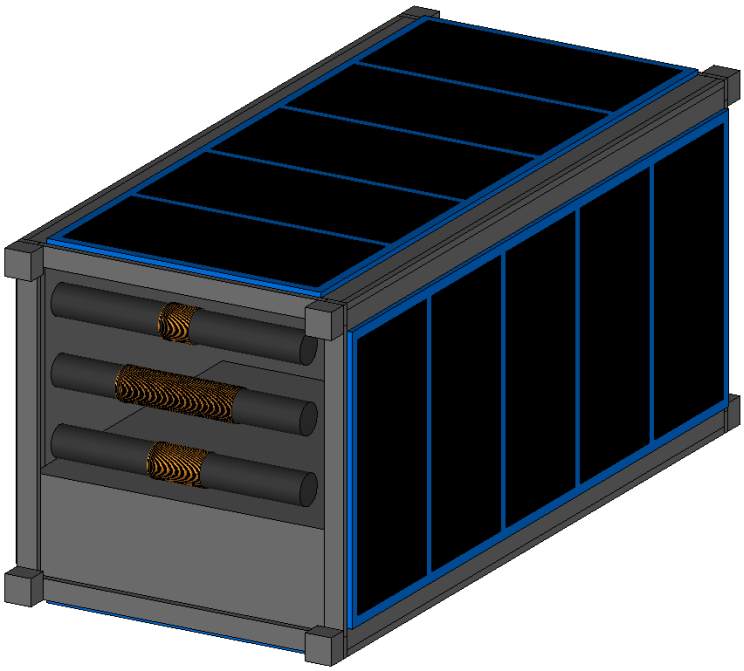

Figure 17: The model satellite in CST MWS used in this work with three ferrite antennas.

Table 6: Simulated coil resistance (R) and reactance (X) for $r_w = 0.15$ mm, N = 10, f = 5 MHz.

K	**R** [Ω]	**X** [Ω]
1.05	0.304	15.1
1.1	0.293	14.9
1.2	0.258	13.8
1.3	0.246	13.8
1.4	0.229	12.7
1.5	0.213	10.4
2	0.182	8.6
3	0.181	7.31
4	0.180	6.29
5	0.148	4.91
10	0.133	5.02
Straight wire	0.103	-

The simulated straight wire corresponds to a situation with no parallel effect. We can see that for a tightly wound coil the proximity effect loss is approximately two times as large as skin effect loss.

4.1.2 Resistance and inductance

Simulations for coil resistances and inductances were done using two different sized ferrite rods (35 × 5 mm and 76.2 × 8.636 mm) and air coils with corresponding coil diameters. The ferrite material was modeled using parameters in table 5. By assuming an idealized equivalent circuit where the antenna impedance consists of only the coil inductance and series resistances their values are simple to determine from the simulated Z-matrix. The frequency at which the values were taken was set to 4 MHz but any other frequency could have been used as the values are compared to the calculated values at the same frequency. In figure 18 the simulation results for two air coils are shown and compared against theoretical calculations in equation (4) and (14) the number of turns N as the variable.

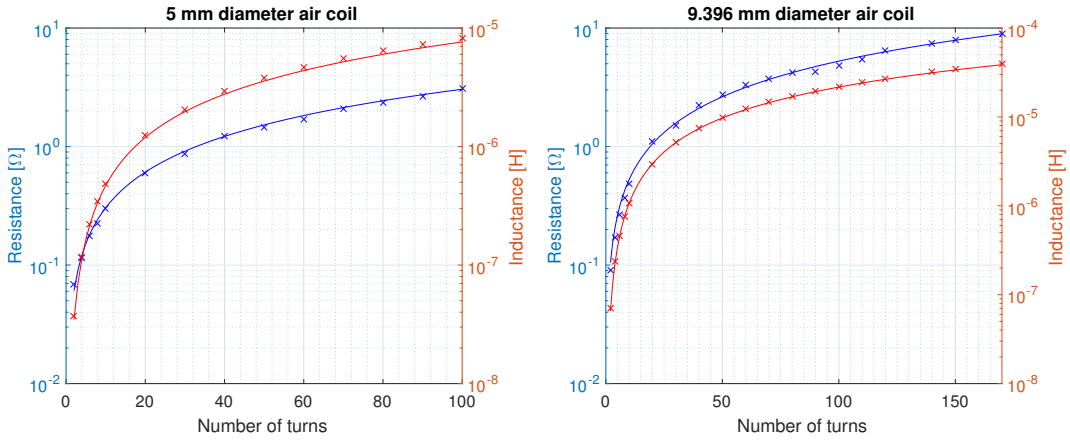

Figure 18: Air loop resistances and inductances for the two simulated coils. The red and blue crosses are the simulated inductance and resistance obtained from CST MWS, respectively. The solid red and blue lines are theoretical values from equation (4) and (14).

The simulated air coil inductance follows accurately the inductance approximation given in 4. The difference from the theoretical inductance is 7 % and 3 % for 100 and 150 turns, respectively. The differences are not very significant considering assumptions and approximations made. The more important fact is that the inductance dependence on the number of turns behaves as expected.

The resistance of the air coil matches the theoretical curve when the increase due to proximity effect R_p/R_0 is set to 2.5 bringing the total resistance to 3.5 times that of no proximity effect. Simulation results in table 6 had a proximity effect which was two times the skin effect resistance.

Figure 19 shows simulation results for the chosen ferrite rod antennas with different number of turns. The figure shows that the inductance of the ferrite rod antennas closely matches the calculated value. This suggests that the ferrite material was modeled correctly by using the CST MWS software and that the coil acts as an inductor. The inductance for the two different rods is 90 % and 97 % of the theoretical value when the coils have 100 turns.

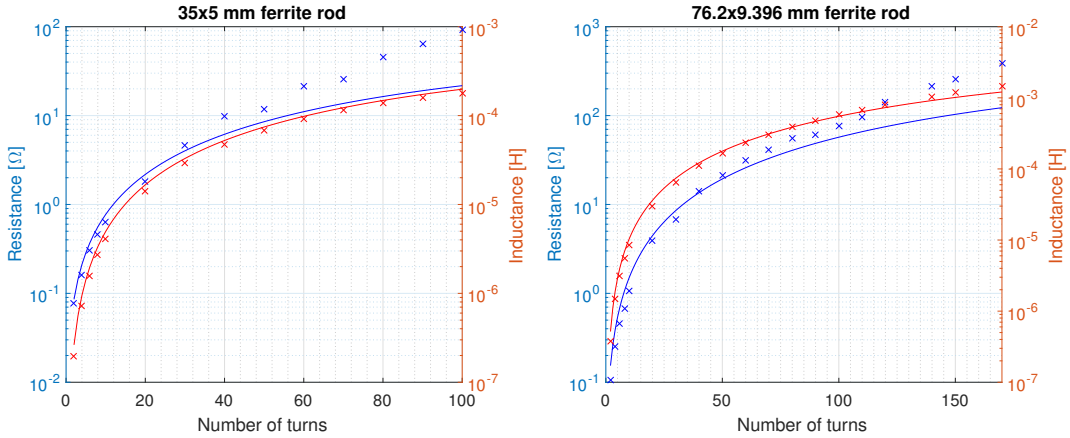

Figure 19: Ferrite rod coil resistances and inductances for the two simulated coils. See figure 18 the description of marks and lines. Theoretical inductance is from equation (5).

The ohmic losses become very high with larger coils and cannot be explained by theoretical skin effect resistance and ferrite core resistance alone. In figure 20 the excess resistance in addition to the skin and proximity effect of an air coil is interpolated and compared to the calculated ferrite losses. In the smaller rod these losses increased more rapidly. The reason for this excess loss can be due to the way the tetrahedral mesh is formed or the simulation is performed when the coil is large. It can also be some real physical process that has been omitted in the analysis. Overall as the results show the simulations seem to give accurate results and as the other processes mentioned earlier are known this excess loss can be isolated if needed.

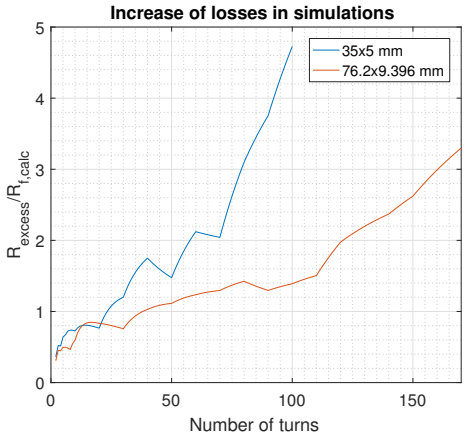

Figure 20: Simulated losses other than skin and proximity effect (R_{excess}) relative to the calculated ferrite losses ($R_{f,calc}$). The blue and red lines represent the two simulated ferrite rod antennas whose dimensions are given in the figure.

In summary the air core simulations matched the theory very well. The increased

ohmic losses can be explained by the proximity effect. In ferrite rod simulations the losses are higher than expected when the coil becomes larger. Further study to determine the origin of these losses is needed but even at this point they don't disqualify the simulation results.

4.1.3 Ferrite rod antenna

Three antennas from table 4 were simulated separately using 16.5 pF parallel capacitance to tune them to 1.5 MHz, 3.0 MHz and 5.0 MHz respectively. The pick-up coil had two turns for every antenna and was placed one wire length away from the main coil like is shown in figure 16. Both plane wave and port excitation were used. Some defining parameters of the antenna are collected in table 7. Both calculated and simulated values are given for each antenna. The resonance frequency is the frequency where the other parameters are calculated or obtained from simulation results.

Table 7: Simulated and calculated antenna parameters. Calculated results are from the frequency response of the antenna using equation (40). Simulation results are from CST MWS.

	Antenna 1		**Antenna 2**		**Antenna 3**	
	Calc.	Sim.	Calc.	Sim.	Calc.	Sim.
f_0 [MHz]	1.495	1.515	3.041	3.041	4.985	5.379
Δf [kHz]	43	45	229	257	744	880
Q	34.8	33.7	13.3	11.8	6.7	6.1
h_e [m]	0.0093	0.0038	0.0098	0.0031	0.0099	0.0028
E($U_{out,min}$)[dBμV/m]	65.68	73.35	65.49	75.13	65.42	75.95
E($U_{out,min}$)[mV/m]	1.92	4.65	1.88	5.71	1.87	6.27

The results show that the resonance frequency and bandwidth from simulations are close to the calculations. The first antenna shows a relatively narrow bandwidth but the other two antennas have a much wider bandwidth. The turn ratio 26:2 for antenna number 3 doesn't decrease the high inductive component of impedance enough for a narrow matching. This is due to two factors: the capacitance range of the varactor and the required minimum signal strength. For example using a smaller rod but with a larger coil in antenna number 3 the bandwidth could be narrowed at the cost of signal level. Similarly the currently used rod in antenna number 3 but with a larger coil and a lower capacitance for the same resonance frequency would produce a narrow bandwidth with the maximum voltage output.

The antenna effective height is similar for all antennas which comes from the signal strength requirement. The calculated effective height is approximately three times the simulated one. The voltage ratio between the main and pick-up coil is slightly lower for simulated antennas. This is because the calculations (c.f. equation (40)) assume a coupling coefficient of 1 between the coils. The additional voltage drop indicates that the coupling coefficients in the simulations were 0.75, 0.85 and 0.85, respectively.

The electric field strength for $U_{out,min}$ means what is the required minimum field strength level for the radio receiver. The minimum level varies approximately between 4 – 6 mV/m.

Table 8: Simulated and calculated antenna parameters with improved matching.

	Antenna 1		**Antenna 2**		**Antenna 3**	
	Calc.	Sim.	Calc.	Sim.	Calc.	Sim.
C_m	1000 pF		500 pF		200 pF	
f_0 [MHz]	1.483	1.508	2.871	2.992	4.828	5.211
Δf [kHz]	6	10	39	50	63	108
Q	247.17	150.80	73.61	59.84	76.63	48.25
h_e [m]	0.0373	0.0123	0.0494	0.0071	0.0987	0.0072
E($U_{out,min}$)[dBμV/m]	53.57	63.22	51.12	67.99	45.11	67.85
E($U_{out,min}$)[mV/m]	0.48	1.45	0.36	2.51	0.18	2.47

To improve the matching a capacitor C_m was added in series with the pick-up coil. Table 8 shows the effect it had on antenna parameters. Using a matching capacitor can be seen to improve the performance of all three antennas. The resonance frequency stays relatively unaffected but the bandwidth is decreased. The effective height of the antennas is increased and the minimum field strength required is 8 – 10 dB less than previously.

4.1.4 Mutual interference

The 76.2 × 8.636 mm rods with identical 70:2 turn ratio for coil windings were used to determine their mutual interference. To get a reference level for resonance and voltage levels a single antenna was simulated alone. The different coil configurations were illustrated in figure 11. The distance between the antenna elements means the distance from antenna center point for parallel configurations. When the antennas are perpendicular to each other the second antenna is rotated 90 degrees and moved so that the antenna center points are now square root of the original distance away from each other.

Table 9 shows how increasing the separation with a perpendicular configuration weakens the interference between the antennas compared to the reference levels. At 30 mm separation (42.4 mm between center points) the effect very noticeable. The signal level is attenuated over 3 dB meaning that more than half of the power is lost. The bandwidth is also more then double than the reference value.

The 30 mm distance was also simulated for all remaining configurations shown in figure 11. The results are shown in table 10. First observation is that when antennas are placed in parallel the mutual interference is almost non-existent. Both configuration number 1 and number 2 have very similar results. Closing the distance between parallel antennas increases the resonance frequency 6 % when the antennas are 10 mm apart. The ferrite rod antenna concentrates magnetic field lines and causes minimal field distortion in parallel elements.

Table 9: Coil test configuration number 3, where the effects of the separation of ferrite antennas from each other was investigated.

Separation [mm]	$U_{out}/U_{out,ref}$ **[dB]**	$f_0/f_{0,ref}$ [%]	$\Delta f_0/\Delta f_{0,ref}$ [%]
30	-3.53	95.6	212.9
40	-0.95	95.6	123.1
50	-0.20	96.7	108.6
60	-0.08	97.0	102.1

Table 10: Two antenna mutual interference. Separation is 30 mm. See figure 11 for illustrations of the coil configurations.

Coil configuration	$U_{out}/U_{out,ref}$ **[dB]**	$f_0/f_{0,ref}$ [%]	$\Delta f_0/\Delta f_{0,ref}$ [%]
1	0.22	97.8	102.6
2	0.20	97.6	102.4
3	-3.53	95.6	212.9
4	-3.57	95.0	212.4
5	-3.39	95.6	226.5
6	-4.25	95.6	232.4

Perpendicular configurations all have very drastic effects compared to parallel ones. All configurations have similar levels of attenuation and widening of the bandwidth. Similar to parallel cases the resonance frequency also drops slightly. Configurations number 3, number 4, and number 5 are more or less equal with minor variations. Configuration number 6 has the highest attenuation and widest bandwidth making it the worst option.

Overall parallel antennas seem to perform better next to each other than perpendicular ones. These are also the worst case scenarios when the antennas are tuned to the same frequency. There are some solutions to minimize mutual interference. One option is to operate antennas in such a way that their resonance frequencies are never close to each other. This can be written in the radio control software measurement modes. This eliminates the possibility to measure same frequency with two antennas.

One solution in minimizing mutual interference is to measure with only one antenna at a time. This can be made by adding a method to disable the antenna RLC circuit such as a switch in series with the coil. The simulations confirm that by making the resonant circuit effectively an open circuit reduces the interference (simulation results not shown). However, using this kind of method increases the complexity in both the circuit and how the antennas are operated. Moreover, simultaneous measurements are then not possible.

4.1.5 Simple satellite body

The prototype measurements conducted with the GTEM cell used a hollow aluminium structure with open ends that had external dimensions of $200 \times 100 \times 100$ mm and a thickness of 2 mm. This was modeled in CST MWS to make the comparison between simulations and measurements possible.

Figure 21 shows how E- and H-fields from an incident plane wave interact with the aluminium structure at 3.33 MHz. The plane wave E-field magnitude is 1 V/m away from the structure. The incident wave is very effectively attenuated and the antenna cannot be positioned very deep into the structure. Also the magnetic field strength is slightly stronger below and above the satellite body. This would suggest that the positions shown in figure 12 outside the satellite might be a worthwhile effort.

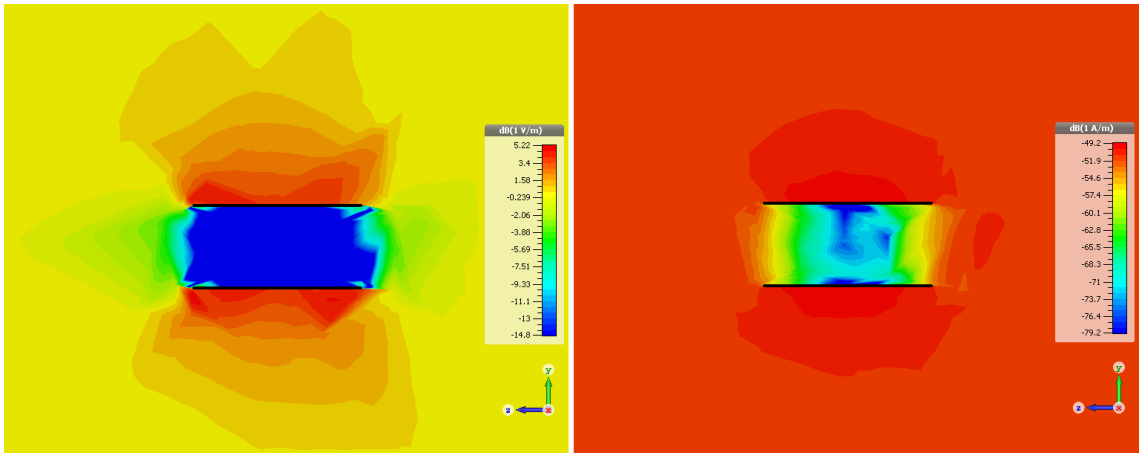

Figure 21: Simulated E-field (left figure, unit dB[1 V/m]) and H-field (right figure, unit dB[1 A/m]) strengths (y- and x-directed respectively) on a 2D-plane at x = 0. The structure was centered at (x,y,z) = (0,0,0) with the long sides along z-axis. E- and H-field were y- and x-directed, respectively. Simulations was made in CST MWS.

Figure 22 shows how the antenna output is attenuated when the antenna is moved inside the metallic body. The edge of the body is at 100 mm where the attenuation relative to free space is approximately 3 dB. The dashed line corresponds to the situation which was measured with the prototype and where the antenna center is 10 mm from the metallic body. The two cases have a similar attenuation curve relative to the z-position but the proximity to the body detunes the antenna resonance.

4.1.6 Antenna position

To determine the usable antenna positions the full model of the satellite shown in figure 17 was used here. The antenna position was swept along the places shown in figure 12. The antenna was placed in the middle of the satellite on x-axis. The antenna used in the simulations was a 35 × 5 mm rod that had 70 turns in the main coil and 2 turns in the pick-up coil in parallel with a 20 pF capacitance. This corresponds to a resonance frequency of approximately 3.3 MHz. The reference level was set on the camera side of the antenna at 105 mm from the satellite center which is where the antennas ends are barely visible from the side. The antenna cannot be placed any further due to constraints set by the launch requirements.

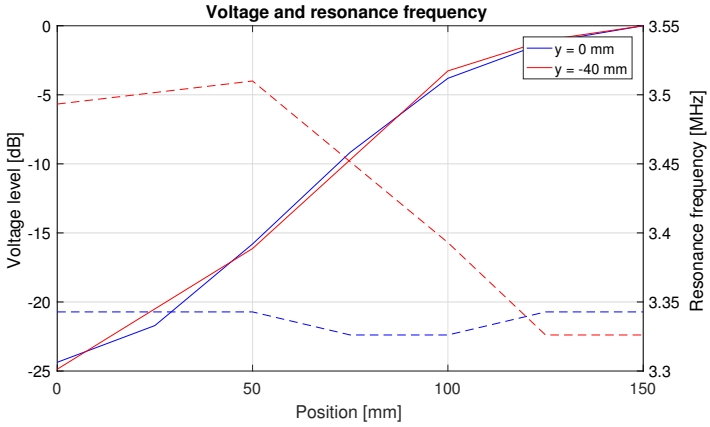

Figure 22: Result of the voltage (full lines) and frequency response (dashed lines) when moving the antenna along z-axis. Positions smaller than 100 mm are inside the aluminium structure. See figure 12 for the z- and y-axis definitions. Simulation was made in CST MWS.

In the analysis several simulations were made in CST MWS to study the response of the antenna. If an extension mechanism is used then the antennas might be placed outside the satellite body approximately 4 cm off the sides (y = ±90 mm) of the satellite. On the camera side by varying the z-position from -60 to -140 mm the voltage gain to the reference level varies 2.2 – 2.9 dB. Similarly, when on the UHF antenna side the z-position was varied between 60 – 140 the voltage gain was 2.4 – 3.0 dB. On the UHF side of the satellite the printed circuit board is at z-level -92.5 mm. When the antenna was placed above the PCB at z-level -100 – -105 mm the signal level was 1.5 – 2.0 dB above the reference level.

On the camera side when the antenna was moved along z-position 100 mm the signal level decreased to -1.5 – 1.4 dB. At z-position 95 mm the level was further reduced to -2.5 – -2.3 dB. Based on these tests the conclusion is that the antenna should be positioned at the maximum allowed level away from the satellite center.

It should be noted that these results do not take into account the interference originating inside the satellite. Placing the antenna outside the satellite gives the best signal level but in addition the interference is reduced as the satellite effectively attenuates signals.

4.1.7 Three antennas with the full satellite model

The chosen three antennas were simulated using the full satellite model. The antenna placement is shown in figure 23. The z-position of the antennas was 100 mm which leaves the antennas half visible from the side. The antenna y-position was set to -5 mm, 15 mm and 35 mm. The order of the antennas was varied and the order which produced the least mutual interference and the most accurate frequency response when the order was 3, 1 and 2 (see table 4) in figure 23 from top to bottom.

The antenna tuning capacitance was set to 16.5 pF which is the same as for the

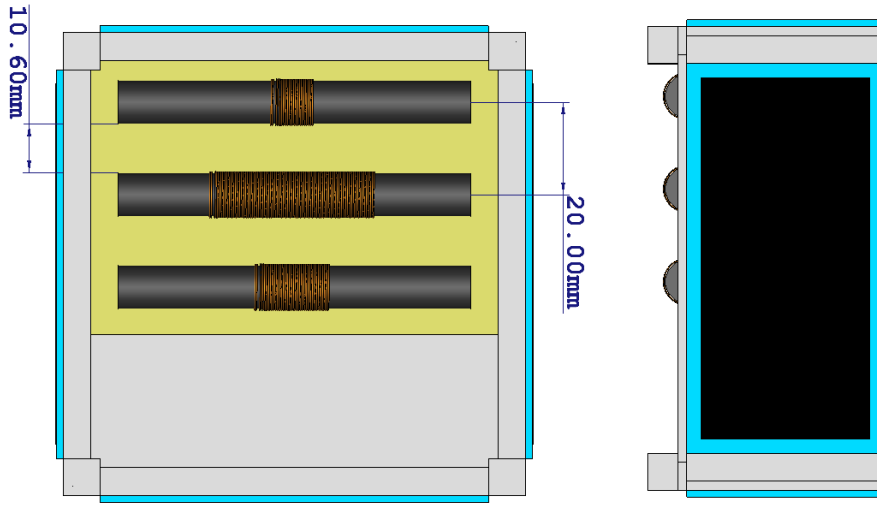

Figure 23: Positioning of the three antennas in the CST MWS simulation.

individual antenna simulations. A plane wave was excited and the output voltages of the antennas were observed. In figure 24 the earlier simulated antenna frequency responses in free-spaces are compared with the measurements where all three antennas are present.

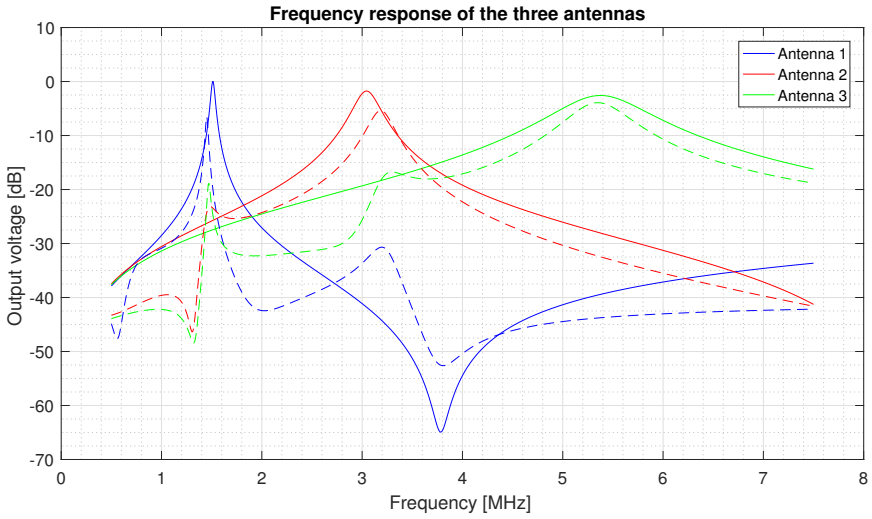

Figure 24: Antenna frequency responses. Full line indicates individual free-space simulations and dashed line simulations with all three antennas at the same time on the satellite.

All three antennas have their voltage output attenuated which means that the minimum receivable field strength is increased. The resonance frequency and the bandwidth are also changed. These are listed in table 11 which can be compared

with the free-space simulations in table 7. The free-space minimum field strength was approximately 4 – 6 mV/m without the matching capacitor C_m. With the satellite and other antennas present the minimum level rises to 7 – 10 mV/m.

Table 11: Antenna parameters with the satellite model when all antennas are used at the same time.

	Antenna 1	**Antenna 2**	**Antenna 3**
f_0 [MHz]	1.452	3.187	5.344
Δf [kHz]	29	255	629
E($U_{out,min}$)[dBμV/m]	79.87	78.75	77.28

4.2 Prototype

Figure 25: Prototype inside an aluminium body next to Si4743 development kit.

To support the simulations a protype was built using a 76.2 × 8.636 mm ferrite rod. The main coil had 80 turns and the pick-up coil 8 turns. From equation (5) the inductance of this coil was calculated to be 416 μH. The copper wire used had a wire radius of 0.15 mm. Figure 25 shows the prototype placed inside a metallic

body. Also shown is a development kit for the radio IC with a BNC connector for the antenna. The development kit enables the testing of the antenna as a part of the radio receiver which is out of scope of this work.

4.2.1 Resonant circuit with four varactors

The prototype was tested using four SMV1251 or SMV1253 varactors in a configuration shown in figure 4. A voltage source was used to input 0 – 8 V voltage to varactor cathodes which according to the datasheets would give a capacitance range of 2.79 – 53.65 pF and 3.28 – 69.32 pF respectively. A signal generator was placed in series with the coil to simulate the induced voltage U_{coil} from an electromagnetic field (U_{coil} in figure 4).

The voltage source was set to a voltage that had a corresponding capacitance given in the datasheet. The signal generators frequency was swept to find the resonance frequency when the antenna output voltage was the highest. By knowing the inductance of the coil the capacitance in the circuit can be determined from equation (2). In figure 26 the capacitance curves for both varactor types are shown.

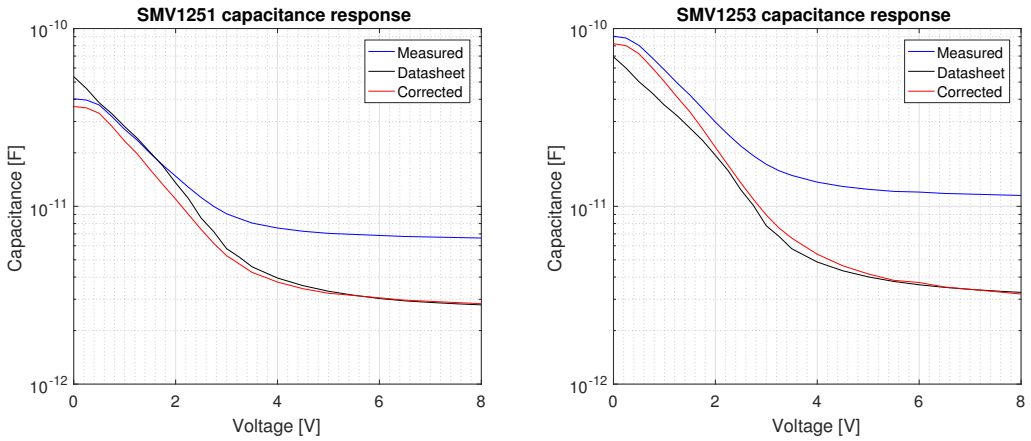

Figure 26: Measured capacitance of the varactors compared to the datasheet values. See text for details.

For both varactors it can be observed that that capacitance value saturates when the voltage is set higher. This is most likely due to parasitic capacitances in the prototype circuit that become larger than the varactor capacitances. The measured curves were corrected by applying a parasitic capacitance of 3.8 pF and 8.3 pF respectively. The corrected curve now accurately gives the same values as in the datasheet when the voltage is high. The high capacitance values are still off but the overall capacitance trend corresponds to the hyperabrupt junction doping profile in equation (51).

The varactor layout behaves as expected by having the correct capacitance isolating the coil from the regulation voltage. Parasitic capacitances in the RLC circuit lower the maximum usable frequency with the varactors. As the capacitance ratio

(highest and lowest capacitance) also decreases, the frequency range of the antenna becomes narrower. This fact needs to be taken into account when manufacturing the actual printed circuit board where the varactors are placed.

In the simulations and for determining the antenna frequency ranges it was assumed that the maximum voltage available for the varactors is 3.3 V. The varactors are capable of even lower capacitance values as shown with higher voltages. Different capacitance ranges are also possible to achieve by simply placing additional varactors in parallel with the four varactors. They must be added in pairs to keep the circuit stabile.

4.2.2 Mutual inductance between the main and pickup coil

The coupling coefficient of the same prototype coil was determined by measuring how the resonance frequency from the main coil output changes depending on whether the secondary pick-up coil was shorted ($Z_L \approx 0\Omega$) or open (Z_L very high). The voltage over the varactors, U_R, was varied to change the capacitance for obtaining several measurement points. Table 12 lists the measured coupling coefficient obtained using equation (38).

Table 12: Measured coupling coefficient. f_o and f_s are resonance frequencies when the pick-up coil is an open and short circuit, respectively.

U_R (V)	f_o (MHz)	f_s (MHz)	k
0.0	1.3	1.45	0.443
0.5	1.3	1.46	0.455
1.0	1.33	1.59	0.548
1.5	1.48	1.79	0.563
2.0	1.61	2.00	0.572
5.0	2.04	2.46	0.559

Calculated inductances of the two coils were 416 μH and 7 μH. From equation (38) the mutual inductance is between 24 – 31 μH. The coupling coefficient is approximately 0.5. This means that the voltage transform is about half of an ideal transformer. Likewise the impedance transform is $1/\sqrt{2}$ compared to an ideal case. The change in impedance can lead to a better matching and a higher voltage output if the decrease in voltage reflection is greater than the decrease in voltage level.

4.2.3 Frequency response

Two 33 pF capacitors were used in parallel to give the antenna a total of 66 pF capacitance. At the measurement point the GTEM cell cavity height (floor to septum) was 30 cm. The input power to GTEM cell was 13 dBm. According to equation (53) this corresponds to electrical field strength of 3.3294 V/m. The frequency response is shown in figure 27. The input impedance of the oscilloscope was 1 MΩ. A corresponding antenna was also simulated in CST MWS.

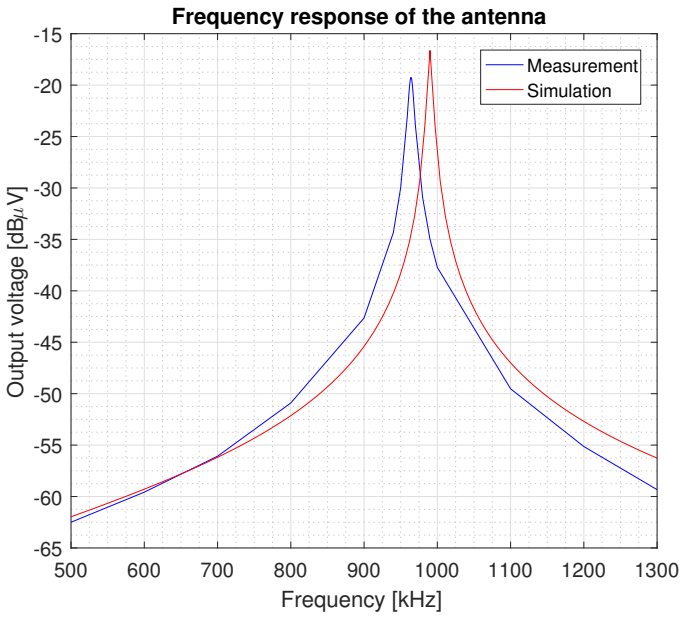

Figure 27: Measured frequency response (blue line) of the single prototype antenna compared with the simulation in CST MWS (red line).

The resonance frequency for the measured antenna was 964 kHz. The output voltage was -19.25 dBV and the bandwidth 8 kHz. In comparison the simulated antenna had a slightly higher resonance frequency at 990 kHz with a 6 kHz bandwidth. The simulation gave -16.64 dBV output voltage, which is 2.61 dB higher then the measured voltage.

The comparison between the measurement and simulation shows that the simulation methods used give accurate results considering the sources of measurement error discussed earlier.

4.2.4 Radiation pattern

The measured radiation pattern from multiple measurements is shown in figure 28. The black solid line is the theoretical radiation pattern of an electrically small antenna ($\sin\theta$). The measurements were done with and without the aluminium body shown in 25 and the measured pattern was unaffected.

The measurements have the predicted trend but the attenuation towards the theoretical null settles to approximately -10 dB. It is possible that something else than the coil in the prototype picked up signal from the electric field. The half-power bandwidth 90 degrees which is expected for an electrically small antenna.

4.2.5 Signal attenuation inside the satellite body

Figure 29 gives the attenuation of the signal when the antenna is moved relative to the satellite. The edge of the metallic body is set at 100 mm. The antenna was

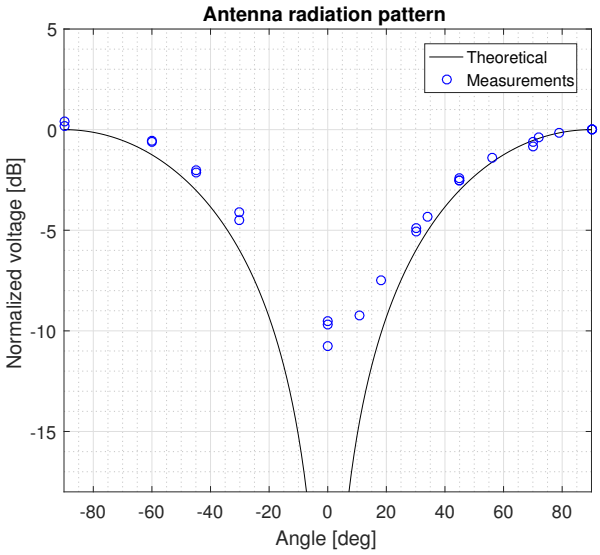

Figure 28: Measured (circles) and theoretical $\sin\theta$ (lines) radiation pattern of the prototype antenna.

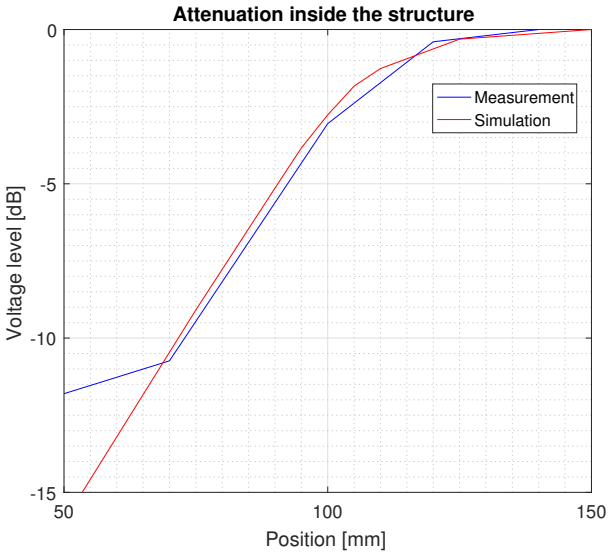

Figure 29: Measured (blue line) and CST MWS simulated (red line) attenuation caused by the metallic structure. Position corresponds to the z-axis position of the antenna (see figure 12).

10 mm off the structure floor. At that point the measured signal relative to free space signal level was -3.05 dB. The measurements can be seen to be in quite well agreement with the simulation results except when at the lowest voltage levels when the antenna is the furthest inside the structure.

5 Summary

In this thesis ferrite rod antennas were studied for Suomi 100 satellite radio instrument operating in the medium and high frequencies measuring radio emissions. The frequency range was specified by the satellite project team from about 1 MHz to 6 MHz. The main steps in the design process were the theoretical analysis of the antenna structure and the simulation of structures derived from theoretical formulas. The simulation process was formed of steps with an increasing complexity to understand the operation of the antenna better and also confirm that the theoretical background is accurate. The simulation results were compared to measurements done with a real prototype antenna. The measurement device used was a GTEM cell which produces a planewave inside the structure. A GTEM cell is an alternative to anechoic chamber tests.

The antennas are designed to receive electromagnetic emissions in general but also AM broadcasts. AM broadcast long distance transmission is highly dependent on ionospheric conditions which determine the propagation path of the signal. The received signals or the absence of them gives information about the opacity of the ionosphere at those frequencies. This way the radio will give information about the ionosphere maximum electron density. AM transmitters have a wide range of transmit powers from a few kilowatts to megawatts. Electric field strength levels from more powerful broadcasts should be expected to be in the range of a few millivolts per meter. This also the required minimum level of field strength that the antennas must be sensitive enough to receive.

The limited space inside and around the Suomi 100 nanosatellite sets limitations to the antenna size. The properties of the used ferrite material enable the ferrite rods to be small enough that they can fit in the satellite. From the latest satellite design a few possible locations for the antennas were explored to determine the effect the satellite has on the antennas and which locations have the best reception.

Three antennas were chosen to cover the requested frequency range. The specific rod and coil size for each antenna gives the highest output voltage in their frequency range. The theoretical formulas were used to iteratively maximize output according to figure 10. Then the structures were modeled in CST MWS simulation software. Simulations were first used to analyze individual components of the equivalent antenna circuit. The simulations confirmed that the coil inductance is accurately predicted in theoretical formulas. For ohmic losses the individual contributions from different loss sources are difficult to determine. Theory provides simple analytical answers to only the skin effect loss and the loss caused by the power absorption in ferrite core. A major loss source is the proximity effect which is difficult to determine analytically and which was observed in the simulations. The simulations also showed an additional loss source that couldn't be attributed to the theoretical losses. It can either be caused by an omitted physical process or an accumulated error in the simulation.

The available ferrite rods are small enough to be used in a nanosatellite. Based on the calculations and simulations sensitive enough antennas can be built. The expected signals levels are weak even from high power transmitters due to the long propagation

path which can be much longer than the direct link between the transmitter and the satellite due to the ionospheric refraction of the signal as a skywave.

The approximate field strength that is measurable by the antennas in free space is 1.4 – 2.5 mV/m. By improving the matching of the antenna this field strength level can be lowered. The simple pick-up coil is an adequate way to match the impedance but additional circuitry can be used. The results show that using a single capacitor for matching improved the output level by 8 – 10 dB. Further improvements in the matching design can be investigated.

Measurements with the GTEM cell confirmed that the results from theory and simulations are in agreement with real ferrite rod antenna measurements. The inductance equation used accurately predicted the real inductance of the built prototype antenna. The frequency response, radiation pattern and the effect of the satellite in both frequency detuning and attenuation follow the theoretical predictions. The measurements validate the used theory and simulation methods. The used electromagnetic simulation software CST MWS can be used for future development in this satellite project. The satellite is still in development and changes in the design are easier to be taken into account by using simulations.

Antenna positioning in the satellite has not yet been finalized. Three areas have been selected that are suitable for a three antenna configuration. Antennas can be placed on either end of the satellite in the free space close to the edge of the satellite body. Another option is to create an extension mechanism that allows the antennas to be extended outside the satellite. If the extension mechanism is not feasible the antennas should be placed in parallel with each other to reduce any possible mutual interference. With the extension mechanism the antennas are far away from each other and any interference is negligible. As the results show there is a meaningful difference in the antenna response in favor of placing them outside the satellite. This option should be kept for future considerations. The main issue is the mechanical complexity of such mechanism. It must be constructed in a way that in the case of a mechanical failure the antennas at all times are positioned in a way that their performance is at an acceptable level. Further studies and designing needs to be conducted for that option to become feasible.

The chosen three antennas fulfill the two main requirements: coverage of the frequency band from approximately 1 to 6 MHz and a sensitivity that is also able to receive strong AM broadcasts. Future development of the antenna should investigate how the upper frequency limit could be extended. For example the EISCAT heater also operates on higher frequencies than the antennas in this work can be tuned to [33].

In the future the whole satellite will and the antenna will undergo standard tests for satellites. These include vacuum and vibration tests. The antenna has to be made of low-outgassing materials. Structurally the antenna and radio have to be secure so that launch vibrations won't damage the instrument or the satellite. In this thesis no supporting structures for the antennas was suggested. Such structures should be designed by using materials that do not affect the antenna performance. In any case the design needs to be revised for any structural changes.

Here three antennas are used to cover the desired frequency band. Three separate

antennas provide some redundancy if for example one of the antennas ceases to operate properly due to mechanical failure although the have different frequency ranges. The frequency coverage can be fulfilled with a single antenna as well. To make a single antenna resonant the required capacitance range is noticeably larger. This can be achieved by using a more sophisticated tuning network than what was used in this work. By using a single antenna the mutual interference issues become non-existent, the mass of the satellite is reduced and the space required for the antenna is also reduced.

References

[1] European Space Agency, "Suomen avaruustoiminnan historiaa." http://www.esa.int/fin/ESA_in_your_country/Finland/Suomen_avaruustoiminnan_historiaa, 2016. Accessed: 2016-10-01.

[2] T. Pulkkinen, S. Merikallio, and P. Stigell, *Space Research in Finland — Report to COSPAR 2014*. Finnish National Committee of COSPAR.

[3] S. Tauriainen, M. Brax, M. Hallikainen, R. Lindgren, J.-P. Luntama, and J. Putkonen, "HUTSAT—A university satellite," *Acta Astronautica*, vol. 38, pp. 707–711, May 1996.

[4] J. Praks, A. Kestilä, M. Hallikainen, H. Saari, J. Antila, P. Janhunen, and R. Vainio, "Aalto-1 — An Experimental Nanosatellite for Hyperspectral Remote Sensing," *Proceedings of IEEE International Geoscience and Remote Sensing Symposium*, pp. 4367–4370, July 2011.

[5] P. Fortescue, G. Swinerd, and J. Stark, eds., *Spacecraft Systems Engineering*. Wiley, 4th ed., 2011.

[6] Suomi 100 -satelliittihanke, "Suomi 100 satelliitti." http://suomi100satelliitti.fi/, 2016. Accessed: 2016-09-10.

[7] International Telecommunications Union, *ITU Radio Regulations*. ITU, 2012.

[8] International Telecommunications Union Radiocommunication Sector, "Frequency Bands allocated to Terrestrial Broadcasting Services." http://www.itu.int/en/ITU-R/terrestrial/broadcast/Pages/Bands.aspx, 2016. Accessed: 2016-09-05.

[9] R. D. Hunsucker and J. K. Hargreaves, eds., *The High-Latitude Ionosphere and its Effects on Radio Propagation*. Cambridge University Press, 2007.

[10] R. Schunk and A. Nagy, *Ionospheres*. Cambridge, 2nd ed., 2009.

[11] J. Mäkelä, *Electromagnetic signatures of lightning near the HF frequency band*. PhD thesis, University of Helsinki, 1999.

[12] Silicon Laboratories, "Si4740/41/42/43/44/45-C10 Automotive AM/FM Radio Receiver," 2009.

[13] A. Nothofer, M. J. Alexander, D. Bozec, A. Marvin, and L. McCormarck, *The use of GTEM cells for EMC measurements*. National Physics laboratory, 2003.

[14] W. L. Stutzman and G. A. Thiele, *Antenna Theory and Design*. Wiley, 3rd ed., 2012.

[15] H. A. Wheeler, "Fundamental Limitations of Small Antennas," *Proceedings of the IRE*, vol. 35, pp. 1479–1484, December 1947.

[16] L. J. Chu, "Physical Limitations of Omni-Directional Antennas," *Journal of Applied Physics*, vol. 19, pp. 1163–1175, May 1948.

[17] H. A. Wheeler, "Simple Inductance Formulas for Radio Coils," *Proceedings of the Institute of Radio Engineers*, vol. 16, pp. 1398–1400, October 1928.

[18] D. B. Miron, *Small Antenna Design*. Newnes, 2006.

[19] Fair-Rite Products Corporation, "Ferrite Components for the Electronics Industry," 2016.

[20] R. C. Pettengill, H. T. Garland, and J. D. Meindl, "Receiving Antenna Design for Miniature Receivers," *IEEE Transactions on Antennas and Propagation*, vol. 25, pp. 528–530, July 1977.

[21] A. M. Urling, V. A. Niemela, G. R. Skutt, and T. G. Wilson, "Characterizing high-frequency effects in transformer windings — a guide to several significant articles," in *Applied Power Electronics Conference and Exposition*, pp. 373–385, April 1989.

[22] D. M. Pozar, *Microwave Engineering*. Wiley, 4th ed., 2011.

[23] G. Smith, "The Proximity Effect in Systems of Parallel Conductors and Electrically Small Multiturn Loop Antennas," tech. rep., Harvard University, December 1971.

[24] Skyworks Solutions, "Varactor Diodes," August 2008.

[25] H. W. Silver, ed., *The ARRL 2016 Handbook for Radio Communications Hardcover*. Amer Radio Relay League, 93rd ed., 2015.

[26] Institute of Electrical and Electronics Engineers, "IEEE Standard for Definitions of Terms for Antennas," *IEEE Std. 145-2013*, March 2014.

[27] E. P. Nichols, *Propagation and Radio Science*. Amer Radio Relay League, 2015.

[28] M. S. Smith, "Non-reversibility for radio rays in the ionosphere," *Journal of Atmospheric Physics and Terrestrial Physics*, vol. 38, pp. 37–44, January 1976.

[29] Amidon Associates, "Amidon Tech Data Book." `http://www.amidoncorp.com/specs/`, 2016. Accessed: 2016-09-25.

[30] Skyworks Solutions, "SMV1247-SMV1255 Series: Hyperabrupt Junction Tuning Varactors," 2016.

[31] E. D. Mantiply, K. R. Pohl, S. W. Poppell, and J. A. Murphy, "Summary of measured radiofrequency electric and magnetic fields (10 kHz to 30 GHz) in the general and work environment," *Bioelectromagnetics*, vol. 18, pp. 563–577, December 1997.

[32] Solar Terrestrial Dispatch, *Proplab-Pro Version 3 Users Guide*, 2016.

[33] EISCAT, "EISCAT's ionospheric Heating facility including Dynasonde." `http://www.eiscat.uit.no/heater.html`, 1993. Accessed: 2016-09-30.

[34] Computer Simulation Technology, "High frequency 3D electromagnetic field simulation software - Frequency Domain Solver." `https://www.cst.com/Products/CSTMWS/Solvers/FrequencyDomainSolver`, 2016. Accessed: 2016-08-11.

[35] Computer Simulation Technology, "RFID Transponder operating at 13.56 MHz." `https://www.cst.com/Applications/Article/RFID-Transponder-Operating-At-1356-MHz`, 2016. Accessed: 2016-09-11.

[36] Computer Simulation Technology, *CST MICROWAVE STUDIO - Workflow and Solver Overview*, 2016.

[37] C. Icheln, "The construction and application of a GTEM cell," Master's thesis, Helsinki University of Technology, 1995.